On the Use of COSMO-SkyMed X-Band SAR for Estimating Snow Water Equivalent in Alpine Areas: A Retrieval Approach Based on Machine Learning and Snow Models

Emanuele Santi, *Senior Member, IEEE*, Ludovica De Gregorio, Simone Pettinato, *Member, IEEE*, Giovanni Cuozzo, *Member, IEEE*, Alexander Jacob, *Member, IEEE*, Claudia Notarnicola, *Member, IEEE*, Daniel Günther, Ulrich Strasser, Francesca Cigna, Deodato Tapete, and Simonetta Paloscia, *Fellow, IEEE*

***Abstract*— This study aims at estimating the dry snow water equivalent (SWE) by using X-band synthetic aperture radar (SAR) data from the COSMO-SkyMed (CSK) satellite constellation. The time series of CSK acquisitions have been collected during the dry snow period in the Alto Adige test site, in the Italian Alps, during the winter seasons from 2013 to 2015 and from 2019 to 2021. The SAR data have been analyzed and compared with the *in situ* measurements to understand the X-band SAR sensitivity to SWE, which has been further assessed by dense media radiative transfer (DMRT) model simulations. The sensitivity analysis provided the basis for addressing the SWE retrieval from the CSK data, by exploiting two different machine learning (ML) techniques, namely, artificial neural networks (ANNs) and support vector regression (SVR). To ensure statistical independence of training and validation processes, the algorithms are trained and tested using SWE predictions of the fully distributed snow model AMUNDSEN as reference data and are subsequently validated on the experimental dataset. Due to its influence on the CSK estimates, the effect of forest canopy was accounted for in the analysis. Depending on the algorithm, the validation resulted in a correlation coefficient $0.78 \leq R \leq 0.91$ and a root-mean-square error (RMSE) 55.5 mm $\leq$ RMSE $\leq$ 87.4 mm between estimated and *in situ* SWE. Further analysis and validation are needed; however, the obtained results seem suggesting the CSK constellation as an effective tool for the retrieval of the dry SWE in alpine areas.**

Manuscript received 2 December 2021; revised 29 April 2022; accepted 20 June 2022. Date of publication 15 July 2022; date of current version 28 July 2022. This work was supported by the Italian Space Agency (ASI) under Grant 2018-37-HH.0. *(Corresponding author: Emanuele Santi.)*

Emanuele Santi, Simone Pettinato, and Simonetta Paloscia are with the Institute of Applied Physics, National Research Council (IFAC-CNR), 50019 Florence, Italy (e-mail: e.santi@ifac.cnr.it).

Ludovica De Gregorio, Giovanni Cuozzo, Alexander Jacob, and Claudia Notarnicola are with the Institute for Earth Observation, EURAC Research, 39100 Bolzano, Italy.

Daniel Günther is with the Zentralanstalt für Meteorologie und Geodynamik (ZAMG), 1190 Vienna, Austria.

Ulrich Strasser is with the Institute for Geography, University of Innsbruck, 6020 Innsbruck, Austria.

Francesca Cigna was with the Italian Space Agency, 00133 Rome, Italy. She is now with the Institute of Atmospheric Sciences and Climate, National Research Council, 00133 Rome, Italy (e-mail: f.cigna@isac.cnr.it).

Deodato Tapete is with the Italian Space Agency, 00133 Rome, Italy (e-mail: deodato.tapete@asi.it).

Digital Object Identifier 10.1109/TGRS.2022.3191409

***Index Terms*— Alpine environment, artificial neural networks (ANNs), COSMO-SkyMed (CSK), machine learning (ML), snow depth (SD), snow water equivalent (SWE), support vector regression (SVR), X-band synthetic aperture radar (SAR).**

I. Introduction

CLIMATE, hydrological, and meteorological studies require an accurate characterization of snow depth (SD) and snow water equivalent (SWE) at a global scale that is, however, unavailable with the characteristics of accuracy, revisiting frequency, and spatial resolution needed by the potential applications. *In situ* systems cannot provide distributed observations at a global scale, and the lack of appropriate sensors hampers the possibility of monitoring the snow cover from space at high resolution. The algorithms based on microwave satellite radiometers [1]–[4] can provide global retrievals of snow mass with frequent revisiting and high accuracy, but with a ground resolution in the order of kilometers that is not sufficient for several applications. On the contrary, the existing synthetic aperture radars (SARs), although more appealing due to the high resolution, do not have optimal frequencies for snow monitoring. The existing satellite SAR sensors operate indeed between the L- and the X-bands, while higher frequencies would be required for this scope. Anyway, some examples of SAR data application for the retrieval of SD and SWE have been published: despite the abovementioned SAR limitations, these studies pointed out some potential of this kind of microwave instrument for the monitoring of snow parameters. Among the others, Guneriussen *et al.* [5] proposed a delta-K technique applied to L-band interferometric SAR (InSAR) for attempting the SWE retrieval. Pettinato *et al.* [6] attempted the SWE retrieval from COSMO-SkyMed (CSK) X-band SAR data, by using an artificial neural network (ANN)-based algorithm, which was trained with data simulated by the dense medium radiative transfer of quasi-crystalline densely packed sticky spheres (DMRT-QCA) forward electromagnetic model [7]. Santi *et al.* [8] exploited a similar combination of dense media radiative transfer (DMRT) simulations and ANN for retrieving SD and SWE from the acquisitions of the European Space Agency's

(ESA) airborne SnowSAR, which is an SAR system operating at X- and Ku-bands in VV and VH polarization. Another example of SWE monitoring from SAR was proposed by Leinss *et al.* [9], [10]: in these studies, the SWE retrieval was obtained by differential interferometry applied to the TerraSAR-X polarimetric acquisitions.

Lievens *et al.* [11] exploited the use of Sentinel-1 C-band SAR data for mapping SD in the Alpine areas of the northern hemisphere: this study is one of the first examples of global SD monitoring based on SAR, although the use of C-band may raise some concerns since this frequency is considered not sensitive to SD due to the very high penetration inside the snow cover [12].

These works show a promising potential of SAR techniques for the monitoring of snow parameters; however, most of the proposed approaches have been validated in relatively small areas and for a limited variability of snowpack conditions, while a consolidated technique for monitoring SD/SWE at global scale by using SAR does not exist yet. It is worth mentioning that a dual-polarized SAR, operating at X-band (9.6 GHz) and Ku-band (17.25 GHz), was foreseen for the Cold Regions Hydrology High-resolution Observatory (CoReH2O) space mission [13], which was proposed in the framework of the 7th Earth Explorer program. The mission, which was aimed at filling the gap of SWE monitoring at high resolution, was not funded by the ESA.

In the absence of a dedicated high-resolution mission, it becomes important to assess the potential of the existing SAR missions operating at the X-band, such as CSK that is building archives of frequent and regular acquisitions. The X-band is still not optimal for the retrieval of SD/SWE; however, this frequency has higher interaction than C-band with the water contained in the snowpack and with the snow microstructure. Furthermore, thanks to the four-satellite constellation, CSK achieves a revisit time up to one day over the same area, which is crucial for snow monitoring applications.

In this study, which was carried out in the framework of ASI-IFAC/CNR "Algoritmi" project [14], a total of about 80 CSK images and corresponding experimental measurements of snow parameters was collected in a large test area corresponding to the South Tyrol, located in the eastern Italian Alps. Images and *in situ* measurements covered the central part of the winter seasons from 2013 to 2015 and from 2019 to 2021. A few reference images collected during the summer period of each year served to verify the absence of wet snow by applying the −3-dB threshold criterion proposed by Nagler and Rott [15] and Nagler *et al.* [16].

First, the X-band sensitivity to SWE of dry snow was analyzed based on the experimental data. The experimental findings were further assessed by DMRT model simulations in quasi-Mie scattering assumption (DMRT-QMS) simulations: the simulated data served for interpreting the experimental findings, with the main scope of answering the very important question whether the data at X-band are sensitive to SWE in the observed environment. The obtained results provided the basis for attempting the SWE retrieval from CSK acquisitions based on ANN and support vector regression (SVR) algorithms.

Given the extension of the test areas and the number of images and winter seasons involved, using DMRT as done in [6] to generate the hundred thousand data required for training the algorithms would have had an unsustainable computational cost. A hybrid "experimental + model"-driven strategy was therefore defined: the training and test of the algorithms were based on subsets of the CSK images combined with SWE simulated by the Alpine MUltiscale Numerical Distributed Simulation Engine [17]. To ensure the statistical independence of validation from training, the dataset derived from the experimental activities was not involved in the training and test phases but only considered for validating the algorithms. The use of AMUNDSEN simulated SWE for training and testing the algorithms, the comparison between different machine learning (ML) techniques, the extension of the test areas, the amount of data, the use of different polarizations, the duration of the experiment, and the assessment of the generalization capabilities represent the main difference and innovation of this study with respect to the preliminary analysis carried out in [6]. In this respect, this study can be considered one of the largest experimental investigations conducted for retrieving SWE from SAR data.

This article's structure is as follows. The South Tyrol test area and the datasets are described in Section II. The main characteristics of the two ML algorithms and their training are described in Section III. In Section IV, the experimental sensitivity of CSK acquisition to SWE is presented and interpreted with the support of DMRT-QMS [18]. The retrieval results are also presented in Section IV and discussed in Section V.

II. Test Area and Data

A. Test Area

The test area considered for the scopes of this study was South Tyrol in the eastern Italian Alps. (Fig. 1), for which a time series of CSK images was available in the winters from 2013 to 2015. The area extension is of about 7400 km^2, and the altitude varies from 200 m to 3905 m a.s.l: such complex orography implies very variable snow conditions throughout the region. Three main topographical landscapes exist in the area: Alpine ridge, Adige valley, and Pre-Alps mountains. These landscapes, together with the Garda Lake, contribute to the large spatial and temporal variability of the snow conditions in the area. The mountain ridges represent a natural obstacle capable to deflect or modify a large-scale weather system. Climate and precipitation amount are indeed strongly influenced by the presence of mountains: while the Adige valley area is characterized by temperate humid conditions, with a mean annual temperature of 11 °C–12 °C, the climate is typically alpine above 1700 m, with mean annual temperatures of 2 °C–3 °C.

The second part of the study focused on a subarea of South Tyrol, the Val Senales, for which another time series of CSK data was available for the winters from 2019 to 2021. Val Senales is a side valley of the Vinschgau (Italian: Val Venosta). The altitude of the valley ranges from about 900 m to 3603 m

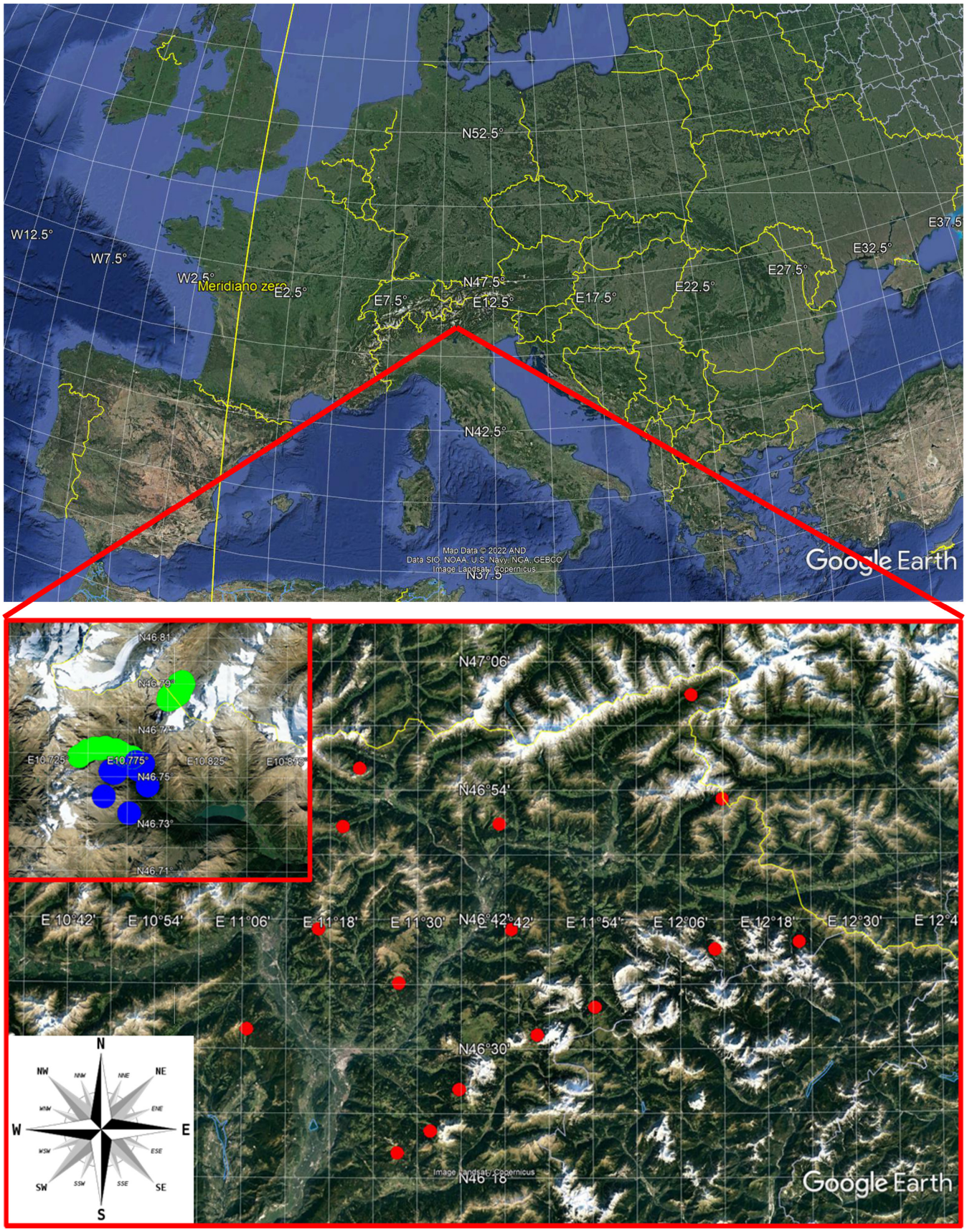

Fig. 1. Test area of Alto Adige with the location of snow measurements collected for the winter 2013–2015 (in red). The box shows a detail of the Val Senales subarea with the location of *in situ* measurements: in green those collected during the winter 2019–2020 and in blue those collected during the winter 2020–2021.

a.s.l. (Similaun peak), thus ensuring the persistence of snow with highly variable conditions for a long part of the year (typically from November to May).

B. In Situ SWE Measurements

For collecting *in situ* SWE measurements to be used as a reference for developing and validating the algorithms, dedicated field campaigns were carried out simultaneously with the satellite overpasses at the locations shown in Fig. 1. In detail, depending on the coverage of CSK images, the *in situ* measurements were collected between 46° and 47°N and 11° and 12.4°E during the winters 2013–2015 (red points in Fig. 1), for a total of 40 data points. In the winter 2019–2020, the *in situ* measurements were collected between 46.75° and 47°N and 10.75° and 11°E (green points in Fig. 1), for a total of 30 data points. Finally, in the winter 2020–2021, the *in situ* measurements were collected between 46.7° and 46.75°N and 10.75° and 10.79°E (blue points in Fig. 1), for a total of 23 data points. In total, 93 SWE *in situ* measurements were collected at the same dates of the CSK acquisitions.

In the first dataset, collected between January and February of the three years (2013–2015), the SWE values ranged from 125 to 670 mm with an average value of 250 mm. In the second dataset, which was collected between November 30, 2019, and March 8, 2021, the SWE values ranged from a minimum of 84 mm to a maximum of 760 mm with an average value of 320 mm. In general, the snow accumulated with the typical alpine behavior, by stratifying during each meteo event with a large variability of the grain size and density from one layer to another. The melting refreezing cycles, which mostly contribute to the snow metamorphism, happen later, in general from the second part of March onward. The different location of *in situ* measurements from one winter season to other hampered, however any consideration about the multiannual trend of snow cover.

The SWE measurements have been obtained by digging a snow pit down to the ground during the field campaigns. The SWE of each layer is measured by using a snow cylinder, and then, the total SWE of the snowpack is calculated as a total of all the layers. Bulk SWE was also measured during the winter 2020–2021 by using a snow tube (Fig. 2). Snow tube measurements are based on the same concept of snow cylinder, but they do not require snow pits, since the measurement is carried out for the entire snowpack.

C. Satellite Data

Two sets of CSK acquisitions were considered for the purposes of this study: the first dataset, obtained from the MAPItaly archive [19], was composed of 25 CSK single-look complex images in HH polarization (HIMAGE mode). The area covered by each image was 40×40 km^2 and the frames were selected to cover the entire South Tyrol. The data were acquired in the central part of the winter seasons (January and February) from 2013 to 2015: this dataset is identified as HIMAGE and served for developing the single-polarization algorithms.

(a) (b)

Fig. 2. (a) Snow tube with a detail of the tip and (b) their use during the field campaigns carried out in Val Senales in 2021.

The second dataset was collected since 2019 according to a specific acquisition plan activated by ASI, to address the needs of the present research. The time series of CSK images were collected over the Val Senales subarea in dual-polarization VV + VH (StripMap PingPong mode—PP) and descending geometry (beam 19), for a total of 50 CSK acquisitions. All the images covered the same frame of 30×30 km^2 and were collected in the winter 2019–2020, from November to March. This dataset is identified as PP2020 and served for developing the dual-polarization algorithms.

Another dataset of four CSK PP images with the same characteristics of the PP2020 dataset was collected in the winter 2020–2021: this dataset is identified as PP2021 and served for evaluating the generalization capabilities of the dual-polarization algorithms.

The SAR images were first preprocessed and calibrated by accounting for the local incidence angle (LIA) in computing actual dimensions of the scattering area for each pixel. During preprocessing, the data were multilooked by selecting the number of looks in range and azimuth corresponding to the desired final spatial resolution and filtered for despeckling using the frost filter with a 5×5 window size [20].

All the images were geocoded using a LiDAR digital elevation model (DEM) at 2.5-m spatial resolution provided by the Bolzano Autonomous Province. The nominal resolution of the SLC input data was 3 m for the HIMAGE images and 15 m for the PP. The final resolution after multilooking and geocoding was 20 m for the HIMAGE and 50 m for the PP: these values were selected according to [21]. Outputs of this preprocessing were the geocoded and calibrated σ°, the LIA, and the layover/shadowing masks. The latter were used to mask out pixels affected by SAR geometric distortion, given the complex orography of the area.

The three datasets used in this study are summarized in Table I, along with the corresponding *in situ* SWE measurements.

D. AMUNDSEN Snow Model

AMUNDSEN [17] is a physically based, distributed snow model, which has been specifically created for modeling

TABLE I
MAIN CHARACTERISTICS OF THE THREE DATASETS USED IN THIS STUDY

Dataset name	HIMAGE	PP 2020	PP 2021
Years	2013-2015	2019-2020	2020-2021
Polarization	HH	VV+VH	VV+VH
Mean incidence	25°-31°	55°	55°
Number of images	25	50	4
in-situ samples	42	35	23

the snowpack in mountain regions characterized by variable climate. AMUNDSEN has been widely validated in the Alpine environment (see [17], [22]–[24]). It provides distributed time series of snow process variables employing a wide range of interpolation, parameterization, and simulation procedures. To simulate accurately the small-scale processes that drive the snow accumulation in alpine terrains, AMUNDSEN requires as input a DEM at tens to hundreds of meters of spatial resolution. The relatively high resolution is necessary for adequately capturing the small-scale processes shaping the snow cover in complex terrain [17]. Other parameters that AMUNDSEN requires as inputs with a temporal frequency from 1 to 3 h are the wind speed, the temperature and relative humidity of the air, the precipitation amount, and the global radiation. Additional inputs, such as land cover, soil, catchment boundaries, and canopy height, are needed to run specific submodules (evapotranspiration, runoff, and snow–canopy interaction). Finally, some topographic parameters, such as the aspect, the slope, the sky-view factor, and the topographic openness/closedness, can be optionally provided to AMUNDSEN for improving the modeling accuracy. The meteorological input data were derived from automatic weather stations of various providers (the University of Innsbruck, Innsbruck, Austria; the Zentralanstalt für Meteorologie und Geodynamik (ZAMG), Vienna, Austria; Avalanche Service Tyrol; Province of Bozen, Meteo Trentino; and EURAC Research, Bolzano, Italy), while land cover was based on the Corine dataset. The complete list of inputs for running the AMUNDSEN simulations and all the details about the model implementation can be found in [17] and [24].

The SWE maps considered here for developing both ANN and SVR algorithms have been obtained by combining AMUNDSEN simulations, *in situ*, and remote sensing data, with the aim of calibrating the AMUNDSEN estimated SWE on *in situ* data as described in [24].

The discrepancies between modeled and measured SWE are not only due to the typical uncertainties of the theoretical models, which are in turn related to the simplifications embedded in any theoretical formulation, but also to errors in driving data, boundary conditions, or structural deficiencies. The method and its performances are detailed in [24]. Overall, a performance improvement with respect to the AMUNDSEN model is evidenced by the decreased root-mean-square error (RMSE) and mean absolute error (MAE) in the validation with *in situ* data.

Distributed maps of SWE at 250-m resolution for the entire region of South Tyrol have been generated using the AMUNDSEN snow model for the dates corresponding to the 25 CSK images available in the HIMAGE mode. AMUNDSEN maps at 50-m resolution have also been generated on the Val Senales subarea for the dates corresponding to the CSK images available in the PP mode during the winters from 2019 to 2020. No further maps have been generated in correspondence of the CSK images collected in 2021, which have been reserved for independent validation of the algorithm.

TABLE II
INPUT RANGE AND STEPS FOR THE DMRT-QMS SIMULATIONS

Frequency/polarizations	9.6 GHz/VV+VH
Incidence angle (ϑ)	From 30° to 60° - 5° step
Number of snow layers	One single layer equivalent
Density (ρ)	From 200 to 400 Kg/m^3 - 50 Kg/m^3 step
Grain size (d)	From 0.8 to 1.6 mm - 0.2 mm step.
Stickiness	0.1
Snow temperature	-10 °C
Snow depth	From 10 to 250 cm – 20 cm step
Soil surface model	Oh
Soil dielectric constant	2.74+j0.14 (frozen soil)
Soil roughness (rms)	1.5 cm

E. DMRT-QMS Model

To better understand the effect of each snow parameter on the CSK acquisitions, the X-band σ° was simulated as a function of the snow parameters and observation geometry by using the DMRT-QMS model [7], [18]. The model implementation used in this study has been developed at the University of Washington: it is freely available and it can be downloaded from the Research Resources webpage of the University of Michigan [25].

The input parameters required by DMRT-QMS are listed in Table II. Among them, the stickiness parameter can relate the scattering properties to the grain shape and snow metamorphism [26].

The backscattering of soil under snow was accounted for by using the Oh model [27]. Model simulations were iterated 2275 times with inputs varying in the range also indicated in Table II.

Upper and lower limits of each input were derived from the experimental measurements. The model simulations shown here are in the same configuration of the CSK PingPong data that mean in VV and VH polarization: the HH polarization exhibited similar behaviors to VV. The dataset obtained in this way has been considered for assessing the experimental findings and understanding the backscattering sensitivity to the main snow parameters and, above all, to SWE. The snow was considered as a single layer, to better point out the effect of each input parameter, and the soil surface under snow was assumed frozen.

F. Ancillary Data

The LIDAR DEM mentioned in Section II-C and a map of forest cover fraction (CF) were also considered in this study. The DEM served not only for geocoding the SAR acquisitions and computing LIA but also as algorithm input. The CF map (from 0% = no forests to 100% = full coverage) had the twofold purpose of identifying the too dense forest, in which the SWE retrieval cannot be performed, and providing an additional input to the algorithms for improving the retrievals in the areas of less dense forest. After some tests, the dense forest threshold has been empirically set to CF = 50%. The relationships between snowpack, topography, and forest coverage have been pointed out in previous studies: among others, Erxleben *et al.* [28] mapped SWE by accounting for the forest coverage and topographic parameters as the aspect, the elevation, and the local slope. Fassnacht *et al.* [29] exploited the SWE dependence on location, aspect, slope, and canopy density.

Both DEM and CF map were resampled and co-registered with the CSK σ°.

III. ML Algorithms Implementation

In recent years, the use of ML for remote sensing applications increased almost exponentially, also due to the progress in computational power of recent computer machines [30]. In this study, two different ML algorithms, namely, ANN and SVR, have been considered for addressing the SWE retrieval from CSK data.

A. ANN Algorithm

ANNs are a statistical method based on minimum variance, which can be applied to solve almost any kind of problem [31], [32]. The ANNs are based on the so-called neuron or perceptron, which was first introduced in the 1950 s with the aim of replicating the working principles of the human brain [33]. ANNs were largely employed in remote sensing. In particular, ANNs have been successfully applied to the soil, vegetation, and snow parameters estimation using SAR data (e.g., [34]–[38]). The capability of easily merging different information sources for addressing the retrieval is one of the main ANNs peculiarities.

The algorithm implemented in this study was based on the ANNs of type feedforward multilayer perceptron (MLP-ANN). In MLP-ANN, a weight is multiplied for each input and a bias is added, and then, the output is moved to each of the neurons in the first hidden layer, where it is added to the other inputs, similarly weighted and biased. The neuron output is then passed through a transfer or activation function and moved to the next layer. Beside the linear function, the most common transfer functions are logistic sigmoid, and hyperbolic tangent, whose output, varies between 0 and 1, and -1 and 1, respectively, for input varying between $-\infty$ and $+\infty$.

The training of MLP-ANN is obtained by iteratively adjusting weight and biases to minimize the mean square error (MSE) between predicted and target values. Such minimization is based on a gradient descendent algorithm known as backpropagation (BP) learning rule.

During training, attention was paid to overfitting: overfitting is a common problem affecting not only ANN but also all the ML algorithms. It occurs when the number of neurons and hidden layers is excessive for the given problem or when the ANN is hypertrained: in the latter case, the ANN learns not only the input–output relationships but also the dataset itself. When overfitting occurs, the ANN can perfectly simulate the training set but fails the retrieval on datasets other than the training set. To prevent overfitting, a systematic search of the optimal architecture for the given problem was implemented [8], [38]: such search led to an architecture composed of two hidden layers with 15 neurons each for the single-polarization algorithm (HIMAGE dataset), and 21 neurons for the dual-polarization implementation (PP datasets). In both implementations, the transfer function was logistic sigmoid, whose output varied between 0 and 1 for inputs varying from $-\infty$ to $+\infty$. Moreover, according to the "early stopping" rule (e.g., [39]), the training set was divided into three subsets composed of 60%, 20%, and 20% of the data: the MSE error on the three subsets was evaluated at each training iteration and the training stopped when the three MSE errors began to diverge.

B. SVR Algorithm

Support vector machine (SVM) is a kind of ML method, which has been developed from the statistical learning theory by Vapnik [40]. SVM algorithms can be divided into two categories: support vector classification (SVC) that is used for classification problems and SVR that is used for regression problems. The latter is a supervised model capable of addressing nonparametric learning: it does not consequently require any assumption about the distribution in the training dataset. As well as ANN, SVR has been widely applied to remote sensing of biophysical variables (e.g., [41], [42]).

The SVR training attempts to find a function $f(x)$ that has at most ε deviation from the target value (yi) for all the training data and is simultaneously as flat as possible [43]. SVR is often used in geo/biophysical variable retrieval mainly because of its capability in handling complex and nonlinear problems and for its ability to manage different kinds of inputs. The capability of handling nonlinear problems is a peculiarity of other nonparametric methods, as the ANN, and parametric ones, as the Bayesian. However, both these approaches require large training sets to obtain robust retrievals. Indeed, ANN and other statistical approaches require to populate the feature space with as many data as possible, for obtaining greater robustness and higher capabilities of interpolation. SVR instead, being based on a geometrical concept, does not require large datasets for training. Indeed, SVR defines a tube of tolerance containing the input data: after identifying the tube limits, the mapping function can be identified based on a small dataset [40]–[43].

During the training phase, the kernel parameters are adjusted, and the algorithm is trained based on the reference input data and the corresponding target values: this process

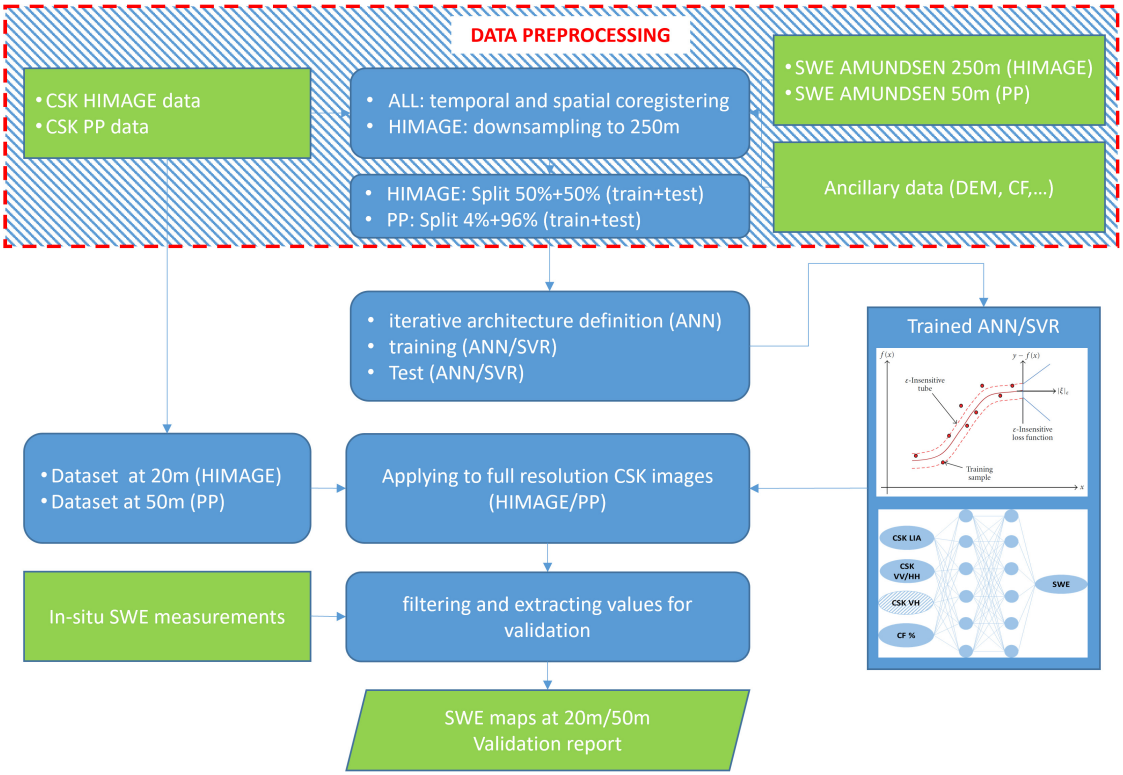

Fig. 3. Flowchart of the training/test and validation process for the HIMAGE and PP (2020 + 2021) datasets. ANN—artificial neural network. CF—forest cover fraction. CSK—COSMO-SkyMed. LIA—local incidence angle. PP—PingPong. SVR—support vector regression. SWE—snow water equivalent.

is called model selection [44]. During the training phase, the SVR algorithm performances are iteratively evaluated on a test dataset, composed of a subset of the training data. Finally, the trained SVR is applied to an independent validation set to assess its performances. The validation completes the training: the obtained regressor can be then used in the operational applications. The SVR described here was based on a Gaussian kernel function, and the maximum number of objective evaluation iterations was set to 30, after testing values from 2 to 100. Increasing the iterations above this number did not improve the accuracy and increase the computational cost, conversely iterating less than 30 times affected the retrieval accuracy.

C. Training, Test, and Validation Strategy

According to the proposed "experimental + model driven" approach, both algorithms were trained by considering the SWE maps simulated by AMUNDSEN as target and validated with *in situ* SWE measurements.

Inputs of ANN and SVR were the calibrated and geocoded CSK backscattering (dB) at the available polarizations, namely, HH for the HIMAGE dataset and VV + VH for the PP (2020 + 2021) datasets, and the corresponding LIA, DEM, and CF map. To comply with the different acquisition modes of CSK, with a single polarization available for HIMAGE and double polarization for PP, and the different spatial resolution of the SWE AMUNDSEN maps (250 m for the HIMAGE dataset and 50 m for the PP datasets), the generation of training and test sets and the algorithm implementation were conducted independently for the HIMAGE and PP datasets. The flowchart of the training, test, and validation process for the HIMAGE and PP datasets is shown in Fig. 3.

1) HIMAGE Dataset: For this subset, the AMUNDSEN maps were available at 250-m resolution: to generate the HIMAGE training and test sets, the CSK σ° in HH polarization, LIA, and CF was resampled at the resolution of the AMUNDSEN map (250 m) and co-registered with SWE on the same grid of coordinates, thus generating a dataset at 250-m resolution containing co-registered σ° HH, LIA, SWE, and CF (in %). The dataset was further divided into two subsets, containing 50% of data each. The first subset was used for training both ANN and SVR, and the second subset was used for testing the algorithms on datasets not involved in the training.

After training with lower resolution data, the ML algorithms were applied to the CSK images for generating the maps of predicted SWE at 20-m resolution. The maps were validated by direct comparison with the *in situ* SWE measurements.

2) PingPong 2020 (PP2020) Dataset: Given the availability of the AMUNDSEN maps at the same resolution of SAR data (50 m), the algorithms developed for the CSK PP collected in the Val Senales were trained using a dataset obtained by sampling the 4% of the combined SAR, AMUNDSEN, and ancillary dataset.

Such sampling rate, which roughly corresponds to one training point every 250 m, was chosen for obtaining training comparable with the one for HIMAGE data. The remaining 96% of the dataset was considered for testing the algorithms, while the validation was again based on the *in situ* data. In this

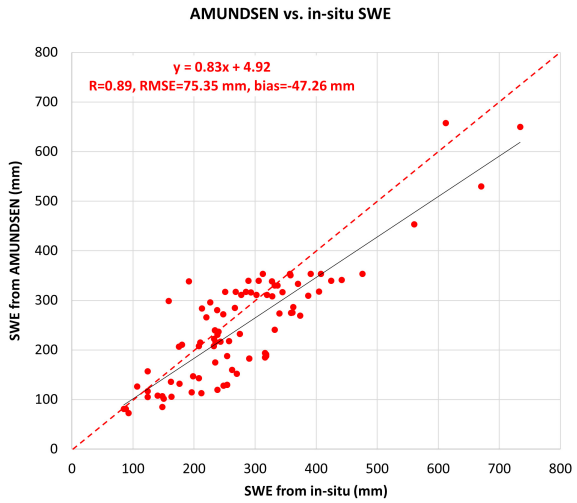

Fig. 4. AMUNDSEN simulated SWE as a function of *in situ* measurements. The gray line is the linear regression, and the dotted red line is the 1:1 line.

case too, the trained algorithms were applied to the entire PP2020 dataset to generate SWE maps at 50-m resolution.

3) Ping Pong 2021 (PP2021) Dataset: The generalization capabilities of the algorithms were evaluated by applying the ANN and SVR trained and tested on the PP2020 dataset to the four CSK images composing the PP2021 dataset, which were not included in the training nor in the test process.

IV. Results

A. AMUNDSEN Model Comparison With in Situ SWE

In this study, the AMUNDSEN simulated SWE served as a reference for training and testing the algorithms.

A comparison between AMUNDSEN simulations and *in situ* measurements has therefore been carried out as a preliminary step for evaluating the accuracy of the AMUNDSEN model, which has been calibrated on other datasets [24], in reproducing the SWE measurements here considered. The result of the comparison carried out on all the 93 *in situ* measurements available is shown in Fig. 4. The AMUNDSEN model was able to simulate the *in situ* SWE with correlation coefficient $R = 0.89$, RMSE $= 75.35$ mm, and bias $= -47.26$ mm, thus confirming its capability of accurate predictions in alpine areas [24].

B. σ° Sensitivity to Dry Snow SWE

In dry snow conditions, previous research [45], [46] pointed out an increase of σ° at the X-band when SWE increases: the trend is more dispersed for shallower SDs, until 50–60 cm, and better correlated with SWE for deeper snow. However, the relationship between σ° and SWE strongly depends on the other parameters that drive the scattering mechanism, namely, the snow density, the grain size, and the observation geometry [8], [46].

1) Model Sensitivity to Snow and Observation Parameters: The σ° sensitivity to the snow parameters and observation angle is represented in Fig. 5: the simulated σ° at both polarizations is shown as a function of SD in Fig. 5(a), the grain size in Fig. 5(b), the snow density in Fig. 5(c), and SWE in Fig. 5(d). The correlation between the simulated backscatter and the incidence (observation) angle is shown in Fig. 5(e). In this case, simulations have been carried out for SD $=$ 130 cm, grain size $= 1.2$ mm, and density $= 250$ kg/m^3.

The plots in Fig. 5 show that σ° is correlated with $0.45 \leq |R| \leq 0.67$ to the first three parameters, with opposite trends: σ° increases with SD and grain size and decreases with snow density. In each plot, the effect of the two parameters other than the target causes an evident dispersion of the data.

Fig. 5(d) shows a decreasing trend when the observation angle increases, with an overall σ° dynamic of about 3/4 dB for ϑ varying between 30° and 60°.

These opposite sensitivities resulted in an average increasing trend of σ° when SWE increases with all the other parameters varying in the range listed in Table II, as shown in Fig. 5(e).

In summary, the analysis carried out using DMRT-QMS pointed out a clear sensitivity of X-band σ° at both polarizations to SWE. However, such relationship is greatly affected by the other snow parameters and the observation geometry, causing the great dispersion pointed out in Fig. 5(e). The dependence on the observation geometry highlights the importance of properly accounting for LIA, especially if the areas are characterized by complex topography, as the South Tyrol.

2) Experimental Sensitivity to SWE: The sensitivity of the CSK observations to SWE was evaluated by direct comparison of σ° acquired by CSK with the spatially and temporally closest *in situ* SWE measurements collected in dry snow conditions. The scatterplot in Fig. 6(a) shows the CSK data in HH polarization (HIMAGE dataset) as a function of the 40 *in situ* SWE measurements collected in the entire South Tyrol between 2013 and 1015. The CSK data in VV + VH polarization (PP2020 + PP2021 datasets) are instead shown against the 53 (30 + 23) *in situ* SWE collected in Val Senales during the winters 2019–2021 in Fig. 6(b) and (c), respectively.

The correlation coefficients were $R = 0.67$ for the HH polarization of the HIMAGE dataset and $R = 0.64$ for the VV polarization of the PP2020 + PP2021 dataset. The VH polarization was found less correlated with SWE: in this case, the experimental relationships resulted in $R = 0.43$.

The regression equations in Fig. 6(b) and (c) were close to those of DMRT simulations shown in Fig. 5(e)

$$\sigma^0_{\text{CSK}} = 3.5 \cdot \log(\text{SWE}) - 36.9$$
$$\sigma^0_{\text{DMRT}} = 2.4 \cdot \log(\text{SWE}) - 24.4$$

for VV polarization and

$$\sigma^0_{\text{CSK}} = 3.4 \cdot \log(\text{SWE}) - 48.3$$
$$\sigma^0_{\text{DMRT}} = 3.5 \cdot \log(\text{SWE}) - 43.5$$

for VH polarization.

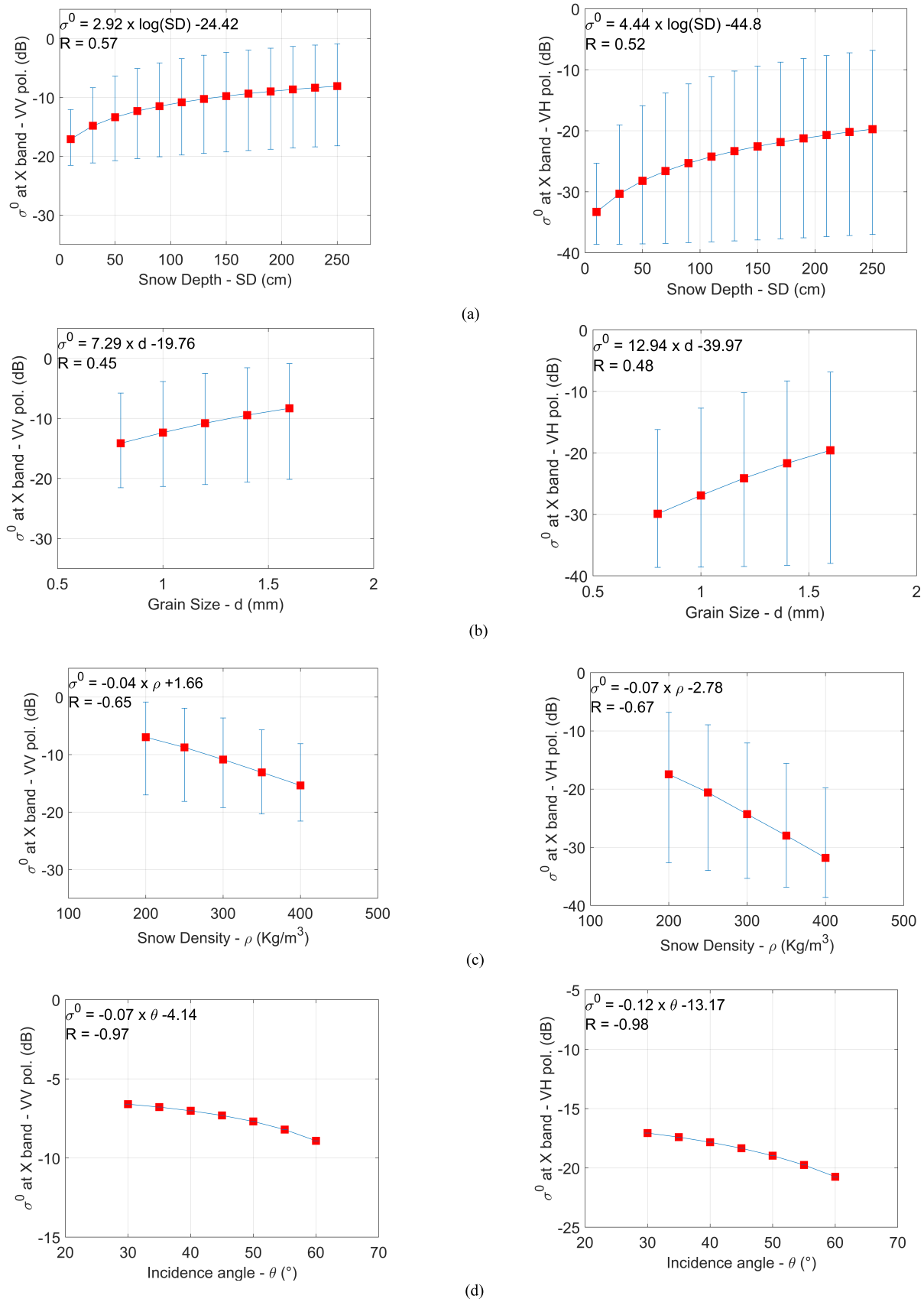

Fig. 5. DMRT simulated backscattering at X-band, VV (on the Left) and VH (on the Right) polarizations as a function of (a) SD, (b) grain size, (c) snow density (ρ), (d) incidence angle (θ), and (e) SWE. The regression equations are reported in the plots.

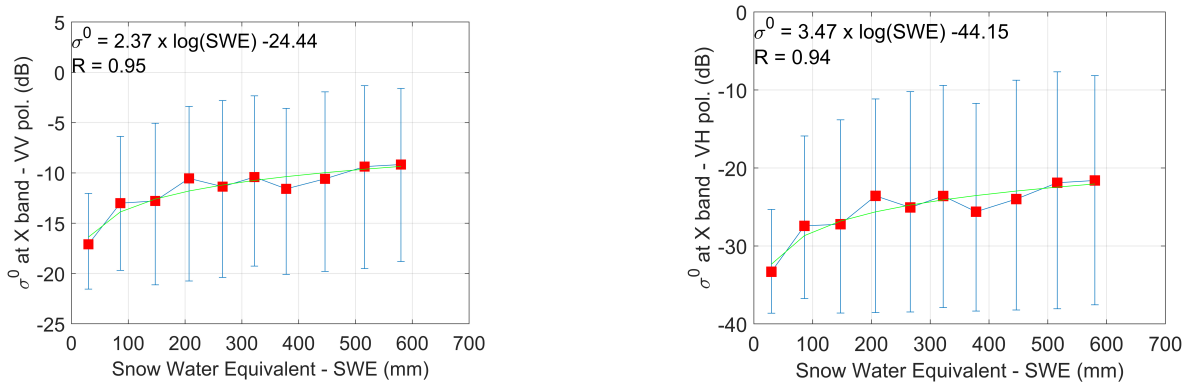

(e)

Fig. 5. *(Continued.)* DMRT simulated backscattering at X-band, VV (on the Left) and VH (on the Right) polarizations as a function of (a) SD, (b) grain size, (c) snow density (ρ), (d) incidence angle (θ), and (e) SWE. The regression equations are reported in the plots.

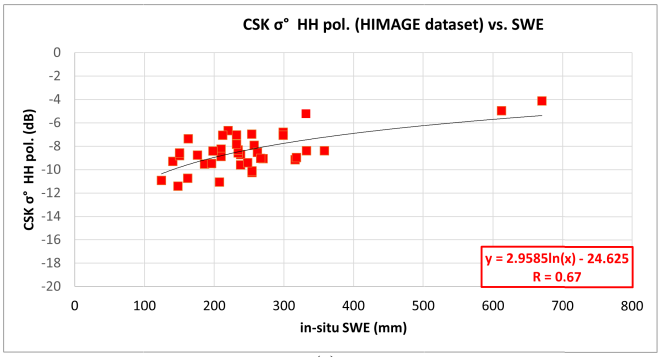

(a)

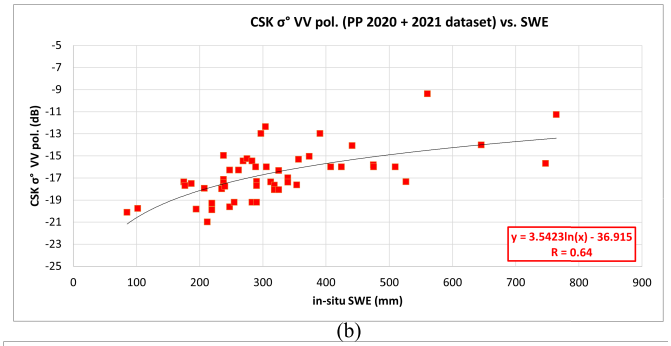

(b)

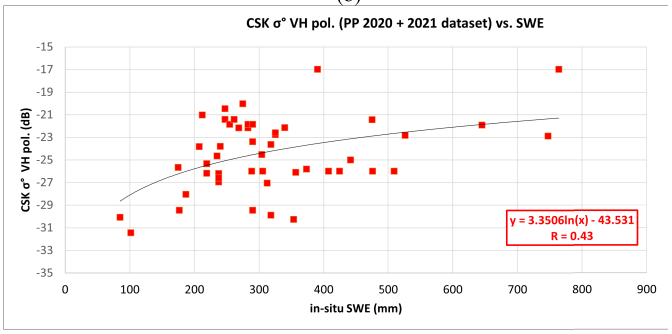

(c)

Fig. 6. CSK σ° as a function of SWE for (a) HIMAGE dataset: HH pol, (b) PP dataset: VV pol, and (c) PP dataset: VH pol.

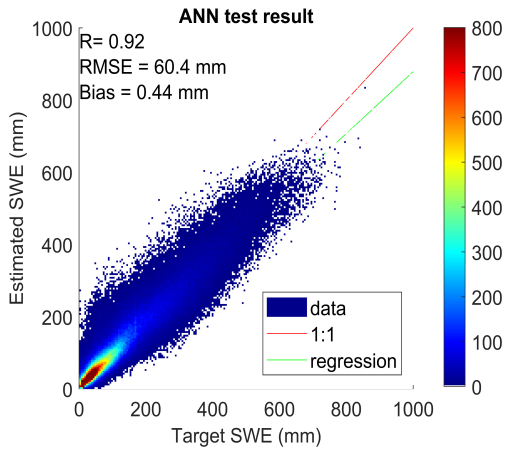

(a)

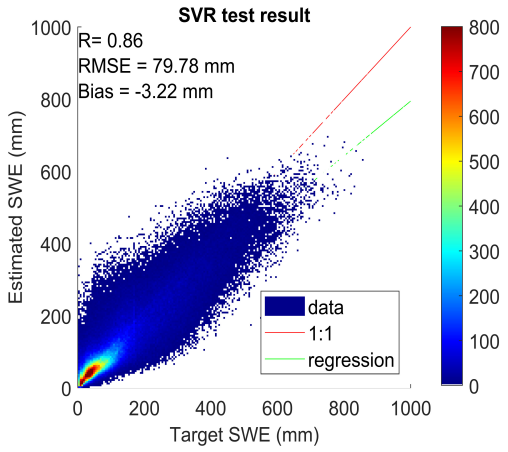

(b)

Fig. 7. Test result for the HIMAGE dataset: density plot of (a) SWE estimated by the ANN and (b) SWE estimated by the SVR, as a function of the target data from AMUNDSEN model simulations. Colors are proportional to the data occurrence.

C. SWE Retrieval ANN/SVR

1) Test Results for the HIMAGE Dataset: The test results, i.e., the output of both algorithms applied to 50% of the HIMAGE dataset not involved in the training, are shown in Fig. 7.

Fig. 7(a) shows the density plot of the SWE estimated by the ANN algorithm as a function of the target SWE from the

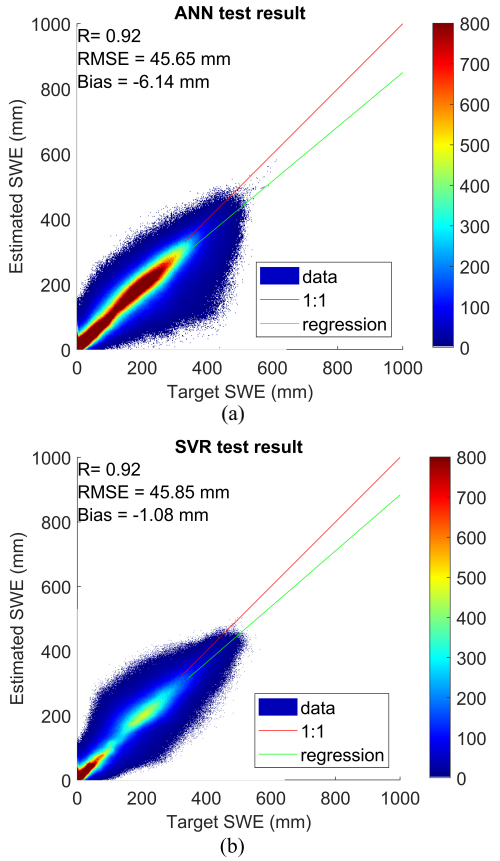

Fig. 8. Test result on the PP 2020 dataset: density plots of (a) SWE estimated by the ANN algorithm and (b) SWE estimated by the SVR algorithm, as a function of the target SWE from AMUNDSEN. Colors are proportional to the data occurrence.

AMUNDSEN maps. Fig. 7(b) shows instead the corresponding result obtained by the SVR. The colorbar is proportional to the data occurrence. The zero SWE values have been discarded to avoid biasing the statistics that are the following: $R = 0.92$ and RMSE $=$ 60.4 mm for ANN and $R = 0.86$ and RMSE $=$ 79.8 mm for SVR. In both cases, the bias was negligible. Despite some small differences in the statistical figures, the overall performances are comparable: this result points out the effectiveness of ML approaches in estimating SWE of dry snow.

2) Test Results for the PP2020 Dataset: The test of both algorithms has been carried out on 96% of the PP2020 dataset not involved in the training (see Section III). Fig. 8(a) and (b) shows the test results as density plots of the SWE estimated by the ANN and SVR algorithms, respectively, as a function of the target SWE from AMUNDSEN simulations.

The ANN algorithm resulted in $R = 0.92$, RMSE $=$ 45.65 mm, and bias $= -6.14$ mm, which is substantially the same result obtained for the HIMAGE dataset. Conversely, the availability of data in double polarization improved considerably the SVR result that obtained results almost identical to ANN, as confirmed by the statistics: $R = 0.92$, RMSE $=$ 45.85, and bias $= -1.08$ mm. In both cases, the result is

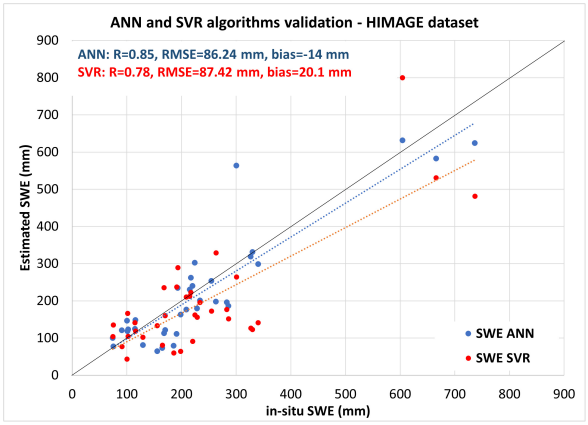

Fig. 9. HIMAGE dataset validation: SWE estimated by the ANN algorithm (blue points) and SWE estimated by the SVR algorithm (red points), as a function of the target SWE from *in situ* measurements.

remarkable since it has been obtained on about 8 million of SWE values by algorithms trained with about 300 000 values.

3) Quantifying the Ancillary Data Contribution: Both algorithms take advantage of the ancillary information provided by the DEM and CF for improving the retrievals. As described in Section III, DEM is used as algorithm input, while the use of CF is twofold: as threshold for forests too dense for attempting the SWE retrieval and as algorithm input for forest below the threshold, which has been established in 50% of the coverage. The effectiveness of using these data has been quantified by repeating the training and test with or without providing them as inputs to the algorithms. In general, the use of the ancillary information raised up the R values of about 8%–10% and decreased the RMSE of about 20%, with small differences depending on the algorithm and dataset. As an example, for the PP2020 dataset, the correlation increased from $R = 0.85$ to $R = 0.92$ and the RMSE decreased from 57 to 45 mm, the latter shown in Fig. 8.

4) Validation Versus in Situ Data: The algorithm validation has been carried out by comparison with the *in situ* data derived from the experimental campaigns: the SWE values estimated by both algorithms have been associated with each *in situ* SWE by applying a minimum distance criterion on the geographical coordinates of the pixel. The results for the HIMAGE dataset are shown in Fig. 9.

The ANN algorithm (blue points in Fig. 9) obtained $R = 0.85$, RMSE $= 86.2$ mm, and bias $= -14$ mm, while the SVR algorithm (red points in Fig. 9) obtained $R = 0.78$, RMSE $= 87.42$ mm, and bias $= 20.1$ mm. The relative error (RE), computed as average of the absolute difference between estimated and target values normalized by the target values, was RE $\simeq$ 20% for ANN and RE $\simeq$ 29% for SVR.

The results in Fig. 9 show that the performances of ANN and SVR are comparable: both methods are capable to exploit the relationship between the CSK measurements and SWE, thus confirming the effectiveness of the proposed methodology.

The validation of PP2020 dataset against the *in situ* measurements collected in Val Senales during the winter

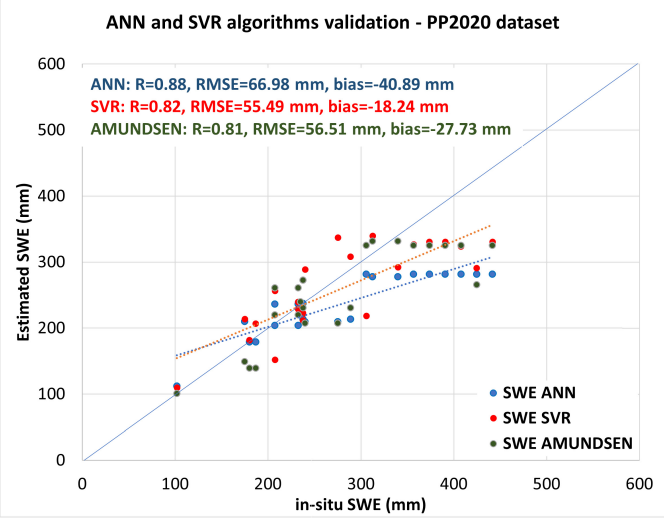

Fig. 10. Validation on the PP2020 dataset: SWE estimated by the ANN algorithm (blue points) and SWE estimated by the SVR algorithm (red points), as a function of the target SWE from *in situ* measurements.

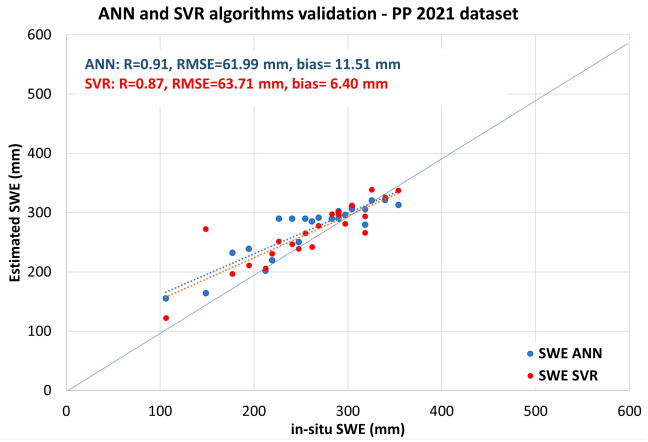

Fig. 11. Validation on the PP2021 dataset: SWE estimated by the ANN algorithm (blue points) and SWE estimated by the SVR algorithm (red points), as a function of the target SWE from *in situ* measurements.

2019–2020 is shown in Fig. 10. The SWE estimated by ANN is shown as red points and the SWE estimated by SVR is shown as blue points. The AMUNDSEN simulations are also shown as dark green points.

The ANN algorithm obtained $R = 0.88$, RMSE $\simeq$ 67 mm, and bias $\simeq -41$ mm, while the SVR obtained $R = 0.82$, RMSE $\simeq$ 56 mm, and bias $\simeq -18$ mm. The RE was RE $\simeq$ 15% for ANN and RE $\simeq$ 14% for SVR.

The ANN slightly outperformed SVR in terms of correlation, and in turn, SVR obtained better RMSE and bias. Therefore, both approaches can be considered substantially equivalent in terms of retrieval accuracy. The results are slightly improved with respect to those obtained for HIMAGE dataset, especially in terms of RMSE and RE, possibly because of the contribution of the second polarization.

It should be mentioned that in this subset, uncertainties exist about the *in situ* SWE values, which in some cases have been computed by using interpolated density values to replace missing measurements: these values differ appreciably from the AMUNDSEN simulations used for training the algorithms. The disagreement is evident from the scatterplot, where a saturation of ANN, SVR, and AMUNDSEN is evident for *in situ* SWE $>$ 300 mm.

On the other hand, both ANN and SVR are highly correlated with the SWE simulated by AMUNDSEN ($R > 0.9$).

5) Generalization Capabilities: The possibility of applying the trained algorithms to other datasets represents, in fact, the main limitation of the retrievals based on ML, especially of the so-called experimental driven approaches, for which the training is based on experimental data only. To verify the generalization capabilities of the proposed retrieval methodology that combines experimental data with AMUNDSEN model simulations, the ANN and the SVR algorithms trained on the PP2020 dataset have been applied to the PP2021 dataset without repeating the training. The results of the comparison with the target SWE are shown in Fig. 11.

The ANN algorithm obtained $R = 0.91$, RMSE $=$ 61.99 mm, and bias $=$ 11.51 mm, while the SVR statistics were $R = 0.87$, RMSE $=$ 63.71 mm, and bias $=$ 6.40 mm. These results are in line with the PP2020 validation shown in Fig. 10: some better agreement can be attributed to the *in situ* SWE derived from bulk measurements obtained by using the snow tube (Section II-B and Fig. 2).

To better evaluate this result, it should be mentioned that the snowpack characteristics varied greatly from a winter season to another. As an example, the absolute difference between SWE for February 3, 2021, and February 2, 2020, is shown in Fig. 12(a), and the corresponding SWE histograms are shown in Fig. 12(b).

The average value of the absolute difference computed on (not zero) SWE is $\simeq$50 mm, and differences up to 270 mm can be observed, especially in the upper part of the map. Moreover, the measurements were collected in areas different from those of 2020, thus increasing the independence of the two datasets. The results in Fig. 11 seem therefore pointing out some spatial and temporal generalization capabilities of the data + model driven approach that a purely experimental-driven approach can be difficult to reach.

6) Comparison With RISC Requirements: An attempt to further quantify these results has been carried out by comparison with the requirements of the RISC Earth Explorer 10 mission proposal, which represents the latest implementation of the CoReH2O retrieval concept. The RISC requirements for SWE product in alpine areas are RMSE $=$ 30 mm for SWE up to 200 mm and a 15% error for SWE $>$ 200 mm. In Fig. 13, the RE (%) between estimated and measured SWE is plotted against the *in situ* data for the PP2021 dataset.

The green line represents the RISK requirement. For convenience, the fixed error below 200 mm has been transformed in RE. Both ANN and SVR show an error decreasing when SWE increases, pointing out a greater retrieval uncertainty, especially for SWE $<$ 150 mm, which agrees with previous findings for X-band SAR [6].

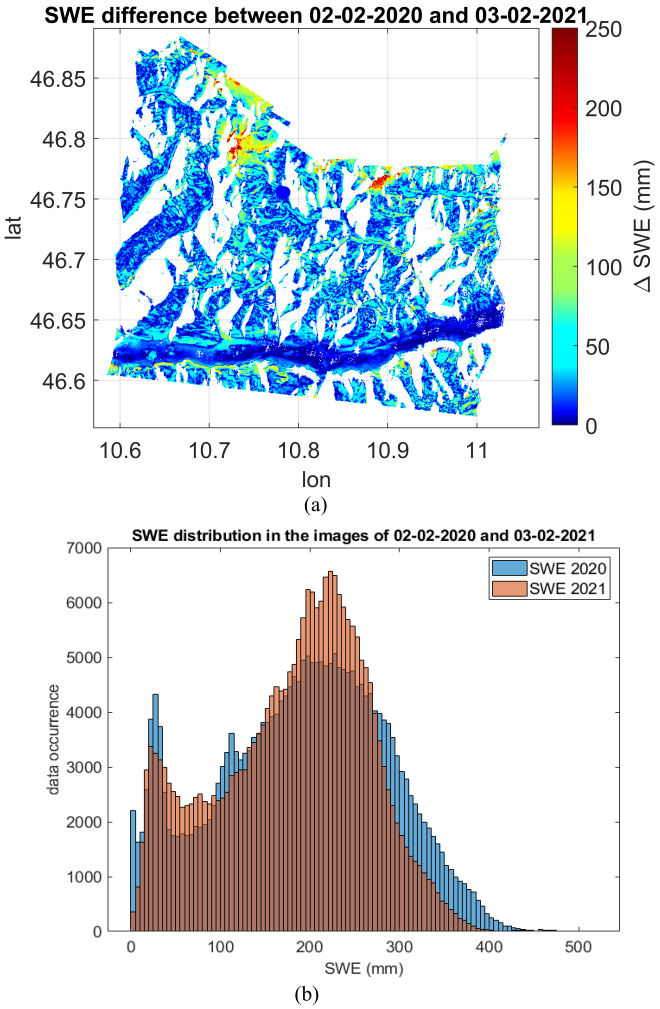

Fig. 12. SWE distributions in the images of February 2, 2020, and February 3, 2021 shown as (a) absolute difference of the SWE maps and (b) SWE distribution histograms.

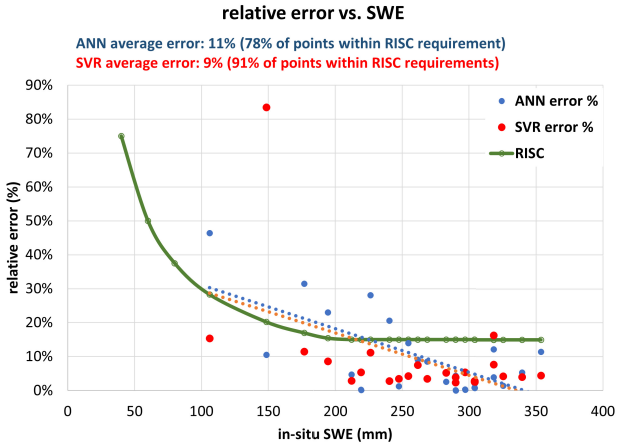

Fig. 13. RE estimated versus target SWE for the PP2021 dataset. Blue points represent the ANN retrievals and red points represent the SVR. The green line is the error limit as established in RISC requirements.

In this analysis, SVR clearly outperformed ANN: 91% of SVR estimated SWE meet the RISC requirement, while only 78% of the ANN estimated SWE is below the green line.

TABLE III
MAIN RESULTS OF THE ANN AND SVR TEST AGAINST AMUNDSEN MODEL SIMULATION AND VALIDATION AGAINST *In Situ* DATA FOR THE BOTH HIMAGE AND PP DATASETS

		Test (vs. AMUNDSEN)		Validation (vs. in-situ)	
		R	RMSE (mm)	R	RMSE (mm)
HIMAGE	ANN	0.92	60.4	0.85	86.2
	SVR	0.86	79.8	0.78	87.4
PP 2020	ANN	0.92	45.7	0.88	57.0
	SVR	0.92	45.9	0.82	55.5
PP 2021	ANN	-	-	0.91	60.0
	SVR	-	-	0.87	63.7

As a side note, it is clear from these comparisons that the "better" retrieval technique depends on the assessment metrics: in general, indeed, the ANN showed better correlation to the target SWE (higher R), while the SVR results showed lower RMSE.

7) SWE Maps: After validating them against *in situ* measurements, both ANN and SVR algorithms have been applied to the entire dataset of CSK images for generating SWE maps of the area covered by the SAR acquisitions. An example of map generated by the ANN is shown in Fig. 14(a), while another example generated by SVR is shown in Fig. 14(b): maps refer to February 2013 and 2015. The SWE maps at 20-m resolution generated by the two algorithms from CSK HIMAGE data are shown on the right of each of Fig. 14(a) and (b), while the corresponding SWE maps from AMUNDSEN are shown on the left. The red points correspond to the positions of the *in situ* measurements.

The wet snow absence was confirmed by the −3-dB threshold criterion proposed by Rott *et al.* [13] and Nagler and Rott [15], which has been applied in comparison to the reference images collected in summer. The time series of air temperature provided by the meteo stations and the information obtained from the *in situ* measurements were also analyzed to support the dry snow assumption.

To facilitate the comparison, the SAR layover and shadowing masks have been applied to the AMUNDSEN maps as well. Beside the quantitative validation described in Sections IV-C1–IV-C6, the SWE estimated by the algorithms appears in agreement with the reference data derived from AMUNDSEN simulations: the lower SWE values are correctly distributed along the valleys and the higher SWE values correspond to the higher altitudes. The same qualitative agreement was found for the other SWE maps that have not been displayed here. No differences between ANN- and SVR-generated maps can be qualitatively identified as well.

Similarly, the results obtained for the PP2020 dataset on the Val Senales subarea are shown in Fig. 15. The maps are referring to November 2019 [Fig. 15(a)] and January 2020 [Fig. 15(b)]: the maps at 50-m resolution derived from CSK are displayed on the right and the corresponding AMUNDSEN maps on the left. The red points show the position of *in situ* measurements. The comparison between AMUNDSEN- and

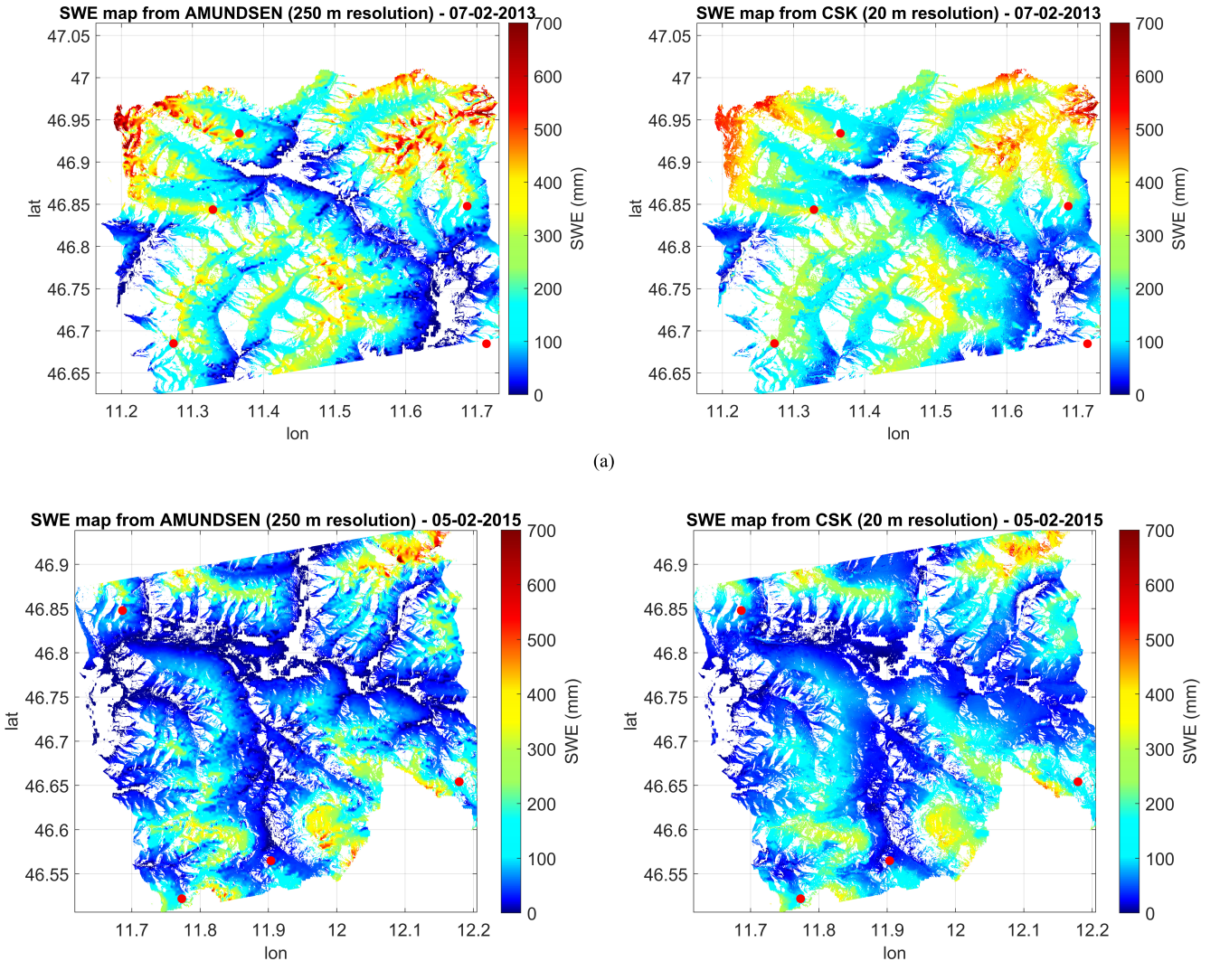

Fig. 14. Examples of algorithm outputs for the HIMAGE dataset obtained by (a) SVR for February 2013 and (b) ANN for February 2015. The SWE maps at 20-m resolution generated from CSK data by the algorithms are displayed on the right and the corresponding AMUNDSEN maps at 250 m are displayed on the left. The colorbar from dark blue to red is proportional to SWE, and layover/shadow areas are in white color. The red points show the position of the *in situ* measurements.

CSK-derived SWE confirms the qualitative good agreement between target and estimated data.

V. Discussion

Table III summarizes the test and validation results shown in Section IV. These results provided a quantitative assessment of the CSK constellation potential in retrieving the SWE of dry snow that was already pointed out in previous studies, but not yet demonstrated with a substantial body of experimental data.

The CSK measurements, either in HH or VV polarization, show a quite good sensitivity to the SWE parameter, provided that the observation geometry is properly accounted for. The test, and especially the validation on independent datasets, pointed out the ability of the proposed methodology in solving the complex relationships that drive the scattering mechanism from snow-covered surfaces, as well as promising spatial and temporal generalization capabilities that the application to the PP2021 dataset of the algorithms trained with the PP2020 dataset seems confirming. In this respect, negligible differences emerged between the ANN and SVR techniques that obtained accuracies comparable with each other. It should be remarked that this study covered several winter seasons between 2013 and 2021, by involving 79 SAR images on a test area of about 7500 km^2, which is characterized by a very complex orography; thus, it represents one of the larger experimental investigations for the monitoring of SWE in Alpine areas carried out by using SAR data. In this respect, the obtained results well support the conclusions about the generalization capabilities of the proposed methodology. Moreover, the use of AMUNDSEN model simulations to train the algorithms had the advantage of extending the representativeness of the snow conditions, by filling the gaps of the experimental datasets

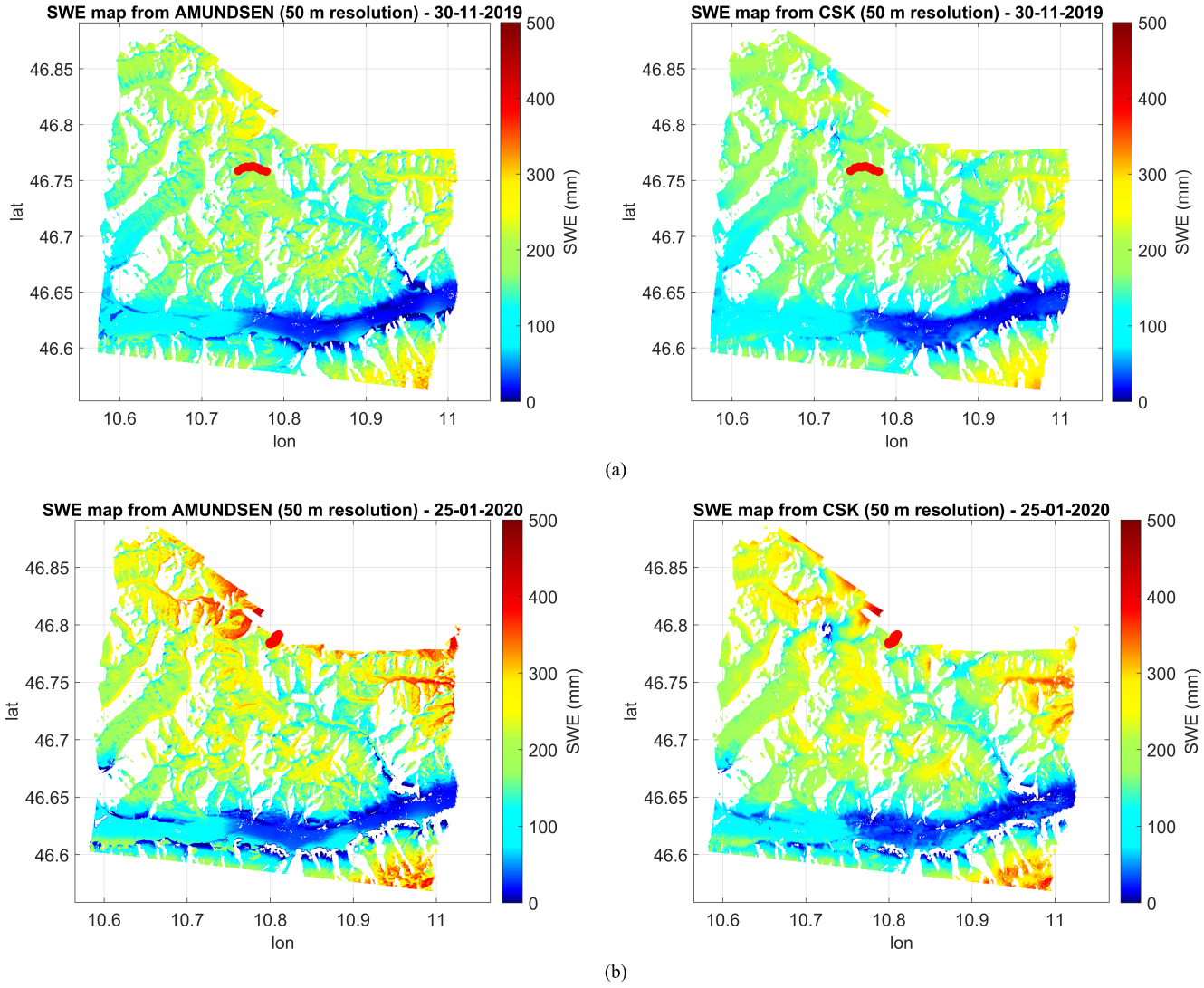

Fig. 15. Example of algorithm outputs for the PP dataset obtained by (a) SVR for November 2019 and (b) ANN for January 2020. The SWE map at 50-m resolution generated by the algorithms is displayed on the right of each image and the corresponding AMUNDSEN maps are displayed on the left. The colorbar from dark blue to red is proportional to SWE, and layover/shadow areas are in white color. The red points show the position of the *in situ* measurements.

and by overcoming the site dependency that is intrinsic of the experimental-driven approaches. It should also be remarked that, given the ML nature of the proposed regressors, the training can be easily updated every time a new dataset is available, without changing the structure of the retrieval algorithm.

The availability of input data, and especially precipitations, could be critical for the snow model simulations on which the training is based (e.g., [47]–[49]). This information is indeed barely available in many locations globally (e.g., [49], [50]); as a result, the methods used here to compute SWE from X-band satellite measurements could not be completed in most places, due to lack of training data. Anyway, the abovementioned generalization capabilities of the algorithms should partially limit this problem: for instance, the dual-polarization algorithms have been trained on 4% of the PP2020 dataset so that three hundred thousand AMUNDSEN simulated SWE values were necessary to estimate SWE over 8 million data points. Moreover, the training was not repeated when applying the algorithms to the PP2021 dataset. In this case, the AMUNDSEN model simulations were not used at all. This could support the algorithm applicability to areas for which a spatially or temporally limited amount of reference SWE data is available.

Another problem that has not been faced in this study is related to the presence of wet snow: in springtime, when snow melting begins, the σ° sensitivity to SWE is lost and wet snow causes a σ° decrease of at least 2–3 dB below the corresponding value of free of snow surfaces [6], [15]. As confirmed by the -3-dB threshold criterion supported by the air and snow temperature information, this condition did not occur in the central part of the winter seasons that have been considered in this study. However, this aspect should be carefully taken into consideration in the case of

operational applications. Further analysis should be (and it will be) therefore conducted for addressing the retrieval in the presence of wet snow.

VI. Conclusion

This study aimed at exploiting the potential of the X-band SAR sensors operating onboard the CSK constellation for monitoring the water equivalent of dry snow (SWE). The analysis focused on the winter seasons between 2013 and 2021 and it was conducted on the South Tyrol region, in the eastern Italian Alps. Time series of data collected by CSK during the dry snow period were compared with the *in situ* measurements of snow parameters collected in dedicated experiments. The experimental sensitivity of SAR acquisitions to snow parameters was further assessed by using the DMRT forward electromagnetic model and the distributed maps of SWE that were generated by using the AMUNDSEN snow model, for the same areas and dates of the satellite acquisitions.

The outcomes of the sensitivity analysis suggested to attempt the retrieval of SWE from the CSK data. Two algorithms based on ML approaches, namely, ANNs and SVR, were therefore implemented, trained, and tested using as a reference the SWE maps simulated by the AMUNDSEN snow model. After training and test, the algorithms were finally validated against the *in situ* SWE from experimental measurements. As ancillary input, the forest CF has been accounted for with the twofold scope to provide a threshold for masking out the dense forest in which the SWE retrieval is not feasible and to be used as ancillary input in the retrieval for compensating the effect of sparse forests on the CSK measurements. The validation of the algorithms against *in situ* measurements resulted in $0.78 \leq R \leq 0.91$ between estimated and target SWE, and 55.5 mm $\leq$ RMSE $\leq$ 87.4 mm, for target SWE values ranging from 0 to 750 mm. These results can be considered encouraging, and they suggest the continuation of the research for exploiting the CSK potential for snow parameter retrieval.

Future works will focus on assessing the effect of wet snow and on extending the validation to other areas and new datasets, to further verify the generalization capability of the proposed methodology. The applicability limits in areas where the *in situ* information required for snow model simulations is missing will be investigated and assessed.

Acknowledgment

This work is carried out by the Institute of Applied Physics, National Research Council (IFAC-CNR), Florence, Italy; EURAC Research, Bolzano, Italy; and the Italian Space Agency (ASI), Rome, Italy, in the framework of the 2019–2022 project "Development of algorithms for estimation and monitoring of hydrological parameters from satellite and drone," under Grant 2018-37-HH.0. COSMO-SkyMed Products were delivered under a license to use by ASI. Snow water equivalent (SWE) monitoring data were kindly provided by the Hydrographic Office of the Province of Bolzano.

References

[1] R. E. Kelly, A. T. Chang, L. Tsang, and J. L. Foster, "A prototype AMSR-E global snow area and snow depth algorithm," *IEEE Trans. Geosci. Remote Sens.*, vol. 41, no. 2, pp. 230–242, Feb. 2003, doi: 10.1109/TGRS.2003.809118.

[2] M. Takala *et al.*, "Estimating northern hemisphere snow water equivalent for climate research through assimilation of space-borne radiometer data and ground-based measurements," *Remote Sens. Environ.*, vol. 115, no. 12, pp. 3517–3529, 2011.

[3] M. Tedesco and J. Jeyaratnam, "A new operational snow retrieval algorithm applied to historical AMSR-E brightness temperatures," *Remote Sens.*, vol. 8, no. 12, p. 1037, Dec. 2016, doi: 10.3390/rs8121037.

[4] M. Tedesco, "NRT AMSR2 unified L3 global daily 25 km EASE-grid snow water equivalent," NASA LANCE AMSR2 GHRC DAAC, 2018, doi: 10.5067/AMSRU/AU_DYSNO_NRT_R01.

[5] T. Guneriussen, K. A. Hogda, H. Johnsen, and I. Lauknes, "InSAR for estimation of changes in snow water equivalent of dry snow," *IEEE Trans. Geosci. Remote Sens.*, vol. 39, no. 10, pp. 2101–2108, Oct. 2001.

[6] S. Pettinato, E. Santi, M. Brogioni, S. Palosica, E. Palchetti, and C. Xiong, "The potential of COSMO-SkyMed SAR images in monitoring snow cover characteristics," *IEEE Geosci. Remote Sens. Lett.*, vol. 10, no. 1, pp. 9–13, Jan. 2013.

[7] L. Tsang, J. Pan, D. Liang, Z. Li, D. W. Cline, and Y. Tan, "Modeling active microwave remote sensing of snow using dense media radiative transfer (DMRT) theory with multiple-scattering effects," *IEEE Trans. Geosci. Remote Sens.*, vol. 45, no. 4, pp. 990–1004, Mar. 2007.

[8] E. Santi *et al.*, "Exploiting the ANN potential in estimating snow depth and snow water equivalent from the airborne SnowSAR data at X- and Ku-bands," *IEEE Trans. Geosci. Remote Sens.*, vol. 60, pp. 1–16, 2021.

[9] S. Leinss, A. Wiesmann, J. Lemmetyinen, and I. Hajnsek, "Snow water equivalent of dry snow measured by differential interferometry," *IEEE J. Sel. Topics Appl. Earth Observ. Remote Sens.*, vol. 8, no. 8, pp. 3773–3790, Aug. 2015, doi: 10.1109/JSTARS.2015.2432031.

[10] S. Leinss, G. Parrella, and I. Hajnsek, "Snow height determination by polarimetric phase differences in X-band SAR data," *IEEE J. Sel. Topics Appl. Earth Observ. Remote Sens.*, vol. 7, no. 9, pp. 3794–3810, Sep. 2014.

[11] H. Lievens *et al.*, "Snow depth variability in the northern hemisphere mountains observed from space," *Nature Commun.*, vol. 10, no. 1, pp. 1–12, Dec. 2019.

[12] C. Mätzler, "Applications of the interaction of microwaves with the natural snow cover," *Remote Sens. Rev.*, vol. 2, pp. 259–387, Jan. 1987.

[13] H. Rott *et al.*, "Cold regions hydrology high-resolution observatory for snow and cold land processes," *Proc. IEEE*, vol. 98, no. 5, pp. 752–765, May 2010.

[14] D. Tapete *et al.*, "Development of algorithms for the estimation of hydrological parameters combining COSMO-SkyMed and Sentinel time series with *in situ* measurements," *IEEE Medit. Middle-East Geosci. Remote Sens. Symp.*, Tunis, Tunisia, Mar. 2020, pp. 53–56.

[15] T. Nagler and H. Rott, "Retrieval of wet snow by means of multitemporal SAR data," *IEEE Trans. Geosci. Remote Sens.*, vol. 38, no. 2, pp. 754–765, Mar. 2000.

[16] T. Nagler, H. Rott, E. Ripper, G. Bippus, and M. Hetzenecker, "Advancements for snowmelt monitoring by means of Sentinel-1 SAR," *Remote Sens.*, vol. 8, no. 4, p. 348, Apr. 2016.

[17] U. Strasser, "Modelling of the mountain snow cover in the Berchtesgaden national park," Berchtesgaden Nat. Park Res. Rep., Berchtesgaden, Germany, Tech. Rep. 55, 2008.

[18] D. Liang, X. Xu, L. Tsang, K. M. Andreadis, and E. G. Josberger, "The effects of layers in dry snow on its passive microwave emissions using dense media radiative transfer theory based on the quasicrystalline approximation (QCA/DMRT)," *IEEE Trans. Geosci. Remote Sens.*, vol. 46, no. 11, pp. 3663–3671, Nov. 2008.

[19] M. L. Battagliere, M. Virelli, F. Lenti, D. Lauretta, and A. Coletta, "A review of the exploitation of the operational mission COSMO-SkyMed: Global trends (2014–2017)," *Space Policy*, vol. 48, pp. 60–67, 2019, doi: 10.1016/j.spacepol.2019.01.003.

[20] F. Argenti, A. Lapini, T. Bianchi, and L. Alparone, "A tutorial on speckle reduction in synthetic aperture radar images," *IEEE Geosci. Remote Sens. Mag.*, vol. 1, no. 3, pp. 6–35, Sep. 2013, doi: 10.1109/MGRS.2013.2277512.

[21] E. Malnes *et al.*, "User requirements for the snow and land ice services—CryoLand," *Cryosphere*, vol. 9, no. 3, pp. 1191–1202, Jun. 2015.

[22] U. Strasser, J. Corripio, F. Pellicciotti, P. Burlando, B. Brock, and M. Funk, "Spatial and temporal variability of meteorological variables at Haut Glacier d'Arolla (Switzerland) during the ablation season 2001: Measurements and simulations," *J. Geophys. Research: Atmos.*, vol. 109, no. D3, pp. 1–18, Feb. 2004.

[23] F. Hanzer, K. Helfricht, T. Marke, and U. Strasser, "Multilevel spatiotemporal validation of snow/ice mass balance and runoff modeling in glacierized catchments," *Cryosphere*, vol. 10, no. 4, pp. 1859–1881, Aug. 2016, doi: 10.5194/tc-10-1859-2016.

[24] L. De Gregorio *et al.*, "Improving SWE estimation by fusion of snow models with topographic and remotely sensed data," *Remote Sens.*, vol. 11, no. 17, p. 2033, Aug. 2019.

[25] (2015). *Research Resources Webpage of the University of Michigan*. [Online]. Available: http://web.eecs.umich.edu/ leutsang/Available Resources.html

[26] H. H. Löwe and G. Picard, "Microwave scattering coefficient of snow in MEMLS and DMRT-ML revisited: The relevance of sticky hard spheres and tomography-based estimates of stickiness," *The Cryosphere*, vol. 9, no. 6, p. 2101, 2015.

[27] Y. Oh, K. Sarabandi, and F. T. Ulaby, "An empirical model and an inversion technique for radar scattering from bare soil surfaces," *IEEE Trans. Geosci. Remote Sens.*, vol. 30, no. 2, pp. 370–381, Mar. 1992.

[28] J. Erxleben, K. Elder, and R. Davis, "Comparison of spatial interpolation methods for estimating snow distribution in the Colorado Rocky Mountains," *Hydrol. Process.*, vol. 16, no. 18, pp. 3627–3649, 2002.

[29] S. R. Fassnacht, K. A. Dressler, D. M. Hultstrand, R. C. Bales, and G. Patterson, "Temporal inconsistencies in coarse-scale snow water equivalent patterns: Colorado river basin snow telemetry-topography regressions," *Pirineos*, vol. 167, pp. 165–185, May 2012, doi: 10.3989/Pirineos.2012.167008.

[30] L. Ma, Y. Liu, X. Zhang, Y. Ye, G. Yin, and B. A. Johnson, "Deep learning in remote sensing applications: A meta-analysis and review," *ISPRS J. Photogramm. Remote Sens.*, vol. 152, pp. 166–177, Jun. 2019, doi: 10.1016/j.isprsjprs.2019.04.015.

[31] K. Hornik, M. Stinchcombe, and H. White, "Multilayer feedforward networks are universal approximators," *Neural Netw.*, vol. 2, no. 5, pp. 359–366, Dec. 1989.

[32] A. Linden and J. Kindermann, "Inversion of multilayer nets," in *Proc. Int. Joint Conf. Neural Netw.*, vol. 2, 1989, pp. 425–430.

[33] F. Rosenblatt, "The perceptron: A probabilistic model for information storage and organization in the brain," *Psychol. Rev.*, vol. 65, no. 6, pp. 386–408, Nov. 1958, doi: 10.1037/h0042519.

[34] N. Baghdadi, S. Gaultier, and C. King, "Retrieving surface roughness and soil moisture from synthetic aperture radar (SAR) data using neural networks," *Can. J. Remote Sens.*, vol. 28, no. 5, pp. 701–711, Oct. 2002, doi: 10.5589/m02-066.

[35] F. Del Frate, P. Ferrazzoli, and G. Schiavon, "Retrieving soil moisture and agricultural variables by microwave radiometry using neural networks," *Remote Sens. Environ.*, vol. 84, no. 2, pp. 174–183, Feb. 2003, doi: 10.1016/S0034-4257(02)00105-0.

[36] S. Paloscia, S. Pettinato, E. Santi, C. Notarnicola, L. Pasolli, and A. Reppucci, "Soil moisture mapping using Sentinel-1 images: Algorithm and preliminary validation," *Remote Sens. Environ.*, vol. 134, pp. 234–248, Jul. 2013.

[37] N. J. Rodríguez-Fernández *et al.*, "Soil moisture retrieval using neural networks: Application to SMOS," *IEEE Trans. Geosci. Remote Sens.*, vol. 53, no. 11, pp. 5991–6007, Nov. 2015, doi: 10.1109/TGRS.2015.2430845.

[38] E. Santi, "Neural networks applications for the retrieval of hydrological parameters from microwave satellite sensors," in *Artificial Neural Networks—Models and Applications Book*. London, U.K.: InTechOpen, 2016, doi: 10.5772/63165.

[39] L. Prechelt, "Early stopping-but when?" in *Neural Networks: Tricks trade*. Berlin, Germany: Springer, 1998, pp. 55–69.

[40] V. N. Vapnik, *The Nature of Statistical Learning Theory*. London, U.K.: Springer, 1999.

[41] L. Bruzzone and F. Melgani, "Robust multiple estimator systems for the analysis of biophysical parameters from remotely sensed data," *IEEE Trans. Geosci. Remote Sens.*, vol. 43, no. 1, pp. 159–174, Jan. 2005.

[42] L. Pasolli, C. Notarnicola, and L. Bruzzone, "Estimating soil moisture with the support vector regression technique," *IEEE Geosci. Remote Sens. Lett.*, vol. 8, no. 6, pp. 1080–1084, Nov. 2011.

[43] A. Smola and B. Schölkopf, "A tutorial on support vector regression," *Statist. Comput.*, vol. 14, no. 3, pp. 199–222, 2014.

[44] L. Pasolli *et al.*, "Estimation of soil moisture in an Alpine catchment with RADARSAT2 images," *Appl. Environ. Soil Sci.*, vol. 2011, pp. 1–12, May 2011.

[45] S. Pettinato, E. Santi, M. Brogioni, S. Paloscia, E. Palchetti, and C. Xiong, "The potential of COSMO-SkyMed SAR images in monitoring snow cover characteristics," *IEEE Geosci. Remote Sens. Lett.*, vol. 10, no. 1, pp. 9–13, Jan. 2013.

[46] S. Paloscia, S. Pettinato, E. Santi, and M. Valt, "COSMO-SkyMed image investigation of snow features in Alpine environment," *Sensors*, vol. 17, no. 1, p. 84, Jan. 2017.

[47] M. P. Clark and A. G. Slater, "Probabilistic quantitative precipitation estimation in complex terrain," *J. Hydrometeor.*, vol. 7, pp. 3–22, Feb. 2006, doi: 10.1175 /JHM474.1.

[48] N. Mizukami and M. B. Smith, "Analysis of inconsistencies in multiyear gridded quantitative precipitation estimate over complex terrain and its impact on hydrologic modeling," *J. Hydrol.*, vol. 428, pp. 129–141, Mar. 2012, doi: 10.1016/j.jhydrol.2012.01.030.

[49] J. Lundquist, M. Hughes, E. Gutmann, and S. Kapnick, "Our skill in modeling mountain rain and snow is bypassing the skill of our observational networks," *Bull. Amer. Meteorol. Soc.*, vol. 100, no. 12, pp. 2473–2490, Dec. 2019, doi: 10.1175/bams-d-19-0001.1.

[50] M. L. Wrzesien, M. T. Durand, and T. M. Pavelsky, "A reassessment of north American river basin cool-season precipitation: Developments from a new mountain climatology data set," *Water Resour. Res.*, vol. 55, no. 4, pp. 3502–3519, Apr. 2019, doi: 10.1029/2018wr024106.

Emanuele Santi (Senior Member, IEEE) received the M.S. degree in electronic engineering from the University of Florence, Florence, Italy, in 1997, and the Ph.D. degree in Earth's remote sensing techniques from the University of Basilicata, Potenza, Italy, in 2005.

Since 1998, he has been a Researcher with the Microwave Remote Sensing Group, Institute of Applied Physics, National Research Council, Florence. He was and is currently involved in many national and international projects funded by the Italian Space Agency (ASI), the European Community (EC), the European Space Agency (ESA), and the Japanese Aerospace Exploration Agency (JAXA), acting as a Team Leader, a WP Leader, and a Co-Investigator. He is in the science team of the NASA's CyGNSS satellite missions since 2019 and in the science team of the ESA's HydroGNSS satellite missions since 2021. He has authored or coauthored 169 papers between ISI books and journals and proceedings of international conferences, by receiving the IEEE J-STARS Paper Prize Award for the best paper published on the IEEE JOURNAL OF SELECTED TOPICS OF APPLIED EARTH OBSERVATIONS AND REMOTE SENSING (J-STARS) in 2017. His research interests include the development and validation of models and statistical inversion algorithms for estimating the geophysical parameters of soil, sea, snow, and vegetation from microwave emission and scattering.

Dr. Santi has been the Conference Chair of SPIE Europe Remote Sensing since 2016. In 2020, he was the Conference Chair of the IEEE 16th Specialist Meeting on Microwave Radiometry and Remote Sensing of the Environment (Microrad 2020). Since 2018, he has been the Vice Chair of the Chapter IEEE GRSS Central North Italy (CNI-29).

Ludovica De Gregorio received the M.S. degree in physics from La Sapienza University, Rome, Italy, in 2013, and the Ph.D. degree in information and communication technologies from the University of Trento, Trento, Italy, in 2019.

Since 2013, she has been working with the Institute for Earth Observation, EURAC Research, Bolzano, Italy, in the framework of different projects dealing with cryosphere. Her research interest includes alpine cryosphere dynamics monitoring with remote sensing data.

Simone Pettinato (Member, IEEE) was born in Florence, Italy, in 1972. He received the M.S. degree in telecommunications engineering from the University of Florence, Florence, in 2002, and the Ph.D. degree in "methods and technologies for environmental monitoring" from the University of Basilicata, Potenza, Italy, in 2007.

In the end of 2013, he has got a permanent position. Since 2003, he has been working at the Microwave Remote Sensing Group, Institute of Applied Physics, National Research Council, Florence, as a Scientist. The objective of his research consists mainly in the investigation of the natural surfaces by means of active and passive microwave sensors in order to retrieve information of geophysical parameters related to the hydrological cycle (soil moisture, snow, and vegetation). He participated, as co-investigator, in different national and international scientific projects funded by the European Community (FLOODMAN and ENVISNOW) and the European Space Agency (GRASS, LEIMON, CORE-H2O, DOMEX-2, DOMEX-3, GPS-SIDS, and GNSS-BIO). In 2009, 2010, and 2012, he was involved in three Antarctic expeditions in order to allow the execution of the DOMEX-2, DOMEX-3, and GPS-SIDS projects, respectively. He was involved in the Italian Space Agency (ASI) projects for floods forecast (PROSA: Satellite Observation Products for Meteorological Alert), COSMO-SkyMed applications (Hydro-Cosmo: the retrieval and monitoring of Land Hydrological parameters for Risk and Water Resources Management), Cap and Trade Assessment by Remote Sensing Investigation (CATARSI), and SIASGE (definition of products at X and X + L bands for SIASGE support). Actually, he is a co-investigator in the regional project (Hydrocontroller) for the monitoring of hydrologic risk and in an international project for sustainable water management for the economic growth and sustainability of the Mediterranean region (OPTIMED-WATER) in the framework of FP7 of European Union. He is also involved in the ASI project METEMW that aims to develop innovative algorithms for the retrieval of hydrological parameters and CRIOSAR for hydrological hazards. He is the author or coauthor of 100 papers published on international peer-reviewed journals and conference proceedings.

Giovanni Cuozzo (Member, IEEE) received the master's degree (*cum laude*) in telecommunication engineering from the University of Federico II, Naples, Italy, in 2003, and the Ph.D. degree in electric engineering and information technology from the University of Cassino, Cassino, Italy in 2007.

From 2006 to 2010, he was a Researcher with the Mediterranean Agency for Remote Sensing and Environmental Control (MARSec), Benevento, Italy, working on near real-time activities related to the satellite receiving station and synthetic aperture radar (SAR) data processing. Since 2010, he has been a Senior Researcher and an Operator of the local satellite ground segment of the EURAC-Institute for Earth Observation, Bolzano, Italy. His research activities are in the field of signal and image processing, especially applied to SAR data with applications in interferometry, soil moisture and biomass retrieval, estimation of biophysical parameters of the cryosphere using machine learning techniques and segmentation of optical and SAR data using Bayesian methods.

Alexander Jacob (Member, IEEE) received the Licentiate degree in geoinformatics from the Royal Institute of Technology, Stockholm, Sweden, in 2014.

He coordinates the research group Advanced Computing for Earth Observation, Institute for Earth Observation, Bolzano, Italy, with the objective to foster EO data science by actively contributing to research in regional and international projects, fully capitalizing on Earth observation (EO) data in the space, time, and feature domains. He is an experienced researcher and a software developer in the field of EO (more than ten years of experience). He is responsible for the scientific data management, including the organization of multidimensional raster data and coordination of algorithm development in operational and research processing chains. He is currently an active project manager for, e.g., Eurac Research's contribution to the Interreg Alpine Space Alpine Drought Observatory project, the ESA openEO platform project, and the ESA SEOM SInCohMap project as well as several internal development projects.

Claudia Notarnicola (Member, IEEE) received the M.S. degree (*summa cum laude*) in physics and the Ph.D. degree in physics from the University of Bari, Bari, Italy, in 1995 and 2002, respectively.

She is currently the Vice-Head of the Institute for Earth Observation, EURAC Research, Bolzano, Italy, where she is also the Leader of a group dealing with remote sensing applications in the synthetic aperture radar (SAR) and optical domain for soil, snow, and vegetation monitoring, as well as integration of remotely sensed observations with models and ground measurements. She conducts research within the frameworks of several national and international projects. Among others, she was also involved in the Cassini–Huygens Mission for the application of an inversion procedure to the estimation of Titan surface parameters. Her research interests include biophysical parameter (soil moisture, vegetation, and snow) retrieval using optical and SAR images, optical and SAR data processing, data fusion, and electromagnetic models.

Dr. Notarnicola has been serving as a Conference Chair for the SPIE International Conference on Microwave Remote Sensing since 2006.

Daniel Günther received the B.Sc. degree in natural sciences and ecohydrology and the M.Sc. degree in hydrology from the University of Freiburg, Freiburg im Breisgau, Germany, in 2012 and 2015, respectively, and the Ph.D. degree from the Department for Geography, University of Innsbruck, Innsbruck, Austria, in 2021.

Since May 2021, he has been a Research Scientist with the Climate Research Department, Zentralanstalt für Meteorologie und Geodynamik (ZAMG), Vienna, Austria, leading the snow modeling team. His key research interests are the numerical simulation of the seasonal snow cover and the integration of remotely sensed information in such modeling frameworks.

Ulrich Strasser received the Habilitation degree from the Department of Geography, University of Munich, Munich, Germany, in 2008.

He worked toward post-doctoral stages with the Centre d'Etudes de la Neige, Grenoble, France, from 1999 to 2000, and the Institute of Hydromechanics and Water Resources Management, ETH Zürich, Zürich, Switzerland, from 2001 to 2002. From 2009 to 2012, he was a Professor of Geography with the Institute for Geography and Regional Science, Graz, Austria. He was a Professor of human-environment system research with the Department of Geography, Faculty of Geo- and Atmosperic Sciences, University of Innsbruck, Innsbruck, Austria, in 2012. He is an internationally recognized, experienced academic teacher and a researcher with a long record of research projects and publications. He has a strong research focus and experience in hydrological modeling in Alpine catchments and profound knowledge in the development of numerical models. He and his group are specialists for the simulation of hydroclimatological processes with a focus on modeling snow conditions in mountain regions and the mass and energy fluxes in the boundary layer between the land surface and the atmosphere.

Francesca Cigna received the B.Sc. and M.Sc. degrees (*cum laude*) in environmental engineering from the University of Palermo, Palermo, Italy, in 2006 and 2007, respectively, and the Ph.D. degree in Earth sciences from the University of Florence, Florence, Italy, in 2011.

She has been a Senior Researcher in Earth observation at the Institute of Atmospheric Sciences and Climate, National Research Council (ISAC-CNR), Rome, Italy, since 2021. She previously worked at the Italian Space Agency (ASI), Rome; the British Geological Survey of the Natural Environment Research Council (BGS-NERC), Keyworth, Nottingham, U.K.; and the University of Florence. Her research interests include satellite synthetic aperture radar (SAR) and optical imagery, advanced interferometric SAR (InSAR) and change detection methods, mapping and monitoring of natural and anthropogenic hazards and risks in urban and rural environments, shallow geological processes, land subsidence, hydrogeology, landscape archeology, and cultural heritage.

Deodato Tapete received the B.Sc. degree (*cum laude*) in mathematics, physics and natural sciences from the University of Florence, Florence, Italy, in 2005, the M.Sc. degree (*cum laude*) in mathematics, physics and natural sciences from the University of Bologna, Bologna, Italy, in 2007, and the Ph.D. degree in Earth sciences from the University of Florence, in 2012.

He is currently a Researcher in Earth observation and data analytics at the Italian Space Agency (ASI), Rome, Italy, a principal investigator of research projects, and the Project Manager of funding contracts with public research bodies and small medium enterprises (SMEs) aimed to development, testing, and prototyping of synthetic aperture radar (SAR) image processing algorithms and derived products. He is involved in the Committee on Earth Observation Satellites (CEOS) and research collaborations in the fields of natural hazards, disaster risk reduction, urban remote sensing, archeology, and cultural heritage.

Simonetta Paloscia (Fellow, IEEE) has been with the National Research Council (CNR), Florence, Italy, since 1984. Since 2004, she has been scientific responsible for the Microwave Remote Sensing Group, Institute of Applied Physics (IFAC), CNR, and the research line "Microwave Remote Sensing of Natural Surfaces," in the EO Project of CNR. In 2010, she was nominated for the Research Director at CNR. She was a Principal Investigator and a Co-Principal Investigator of many national and international projects [the Italian Space Agency (ASI), the European Community (EC), the European Space Agency (ESA), and the Japan Aerospace and Exploration Agency (JAXA)]. Since 1996, she has been a Principal Investigator in the JAXA Science Team of AQUA/AMSR-E and GCOM/AMSR-2 for algorithms' development of soil moisture and vegetation biomass retrieval. She is the author or a coauthor of more than 100 works published in international journals and books and more than 200 articles published on proceedings of international meetings. Her research focuses on the study of microwave emission and scattering of soil (bare and snow-covered) and vegetation.

Dr. Paloscia was a member of organizing and steering committees of international meetings (Specialist Meeting on Microwave Radiometry and International Geoscience and Remote Sensing Symposium). She is a member of the Soil Moisture Active Passive (SMAP) JPL/NASA Science Team. She is also a member of the Permanent Steering Committee of MicroRad Meeting and the General Co-Chair of the MicroRad 1999 and 2008 and URSI-F 2010 Meetings organized in Florence. She has been a URSI Fellow since 2020. She was the Vice-Chair and the Chair of the URSI Commission F from 2011 to 2017. She is an Associate Editor of the *International Journal of Remote Sensing*, IEEE JOURNAL OF SELECTED TOPICS IN APPLIED EARTH OBSERVATIONS AND REMOTE SENSING (IEEE J-STARS), and *European Journal of Remote Sensing*.

Open Access funding provided by 'Consiglio Nazionale delle Ricerche' within the CRUI CARE Agreement